Journal of Molecular Liquids 414 (2024) 126175

Contents lists available at ScienceDirect

Journal of Molecular Liquids

journal homepage: www.elsevier.com/locate/molliq

Harnessing nano-synergy: A comprehensive study of thermophysical characteristics of silver, beryllium oxide, and silicon carbide in hybrid nanofluid formulations

Hamza Babar [a,*], Hongwei Wu [a,*], Wenbin Zhang [b], Yongqi Xie [c]

[a] School of Physics, Engineering and Computer Science, University of Hertfordshire, Hatfield AL10 9AB, United Kingdom
[b] School of Science and Technology, Nottingham Trent University, Clifton Lane, Nottingham NG11 8NS, United Kingdom
[c] School of Aeronautic Science and Engineering, Beihang University, Beijing 100191, China

ARTICLE INFO

Keywords:
Heat transfer
Nanofluids
Stability
Surfactant
Thermophysical properties

ABSTRACT

Nanofluids, promising to improve heat transfer efficiency, encounter stability and durability challenges, hindering their industrial applications. The emerging concept of hybrid nanofluids, alongside surfactant-driven stability research, presents a promising solution to tackle challenges in heat transfer, potentially revolutionizing thermal management systems and advancing nanomaterial science. This comprehensive study investigates the thermophysical properties of simple and hybrid nanofluid formulations composed of silver (Ag), beryllium oxide (BeO), and silicon carbide (SiC) nanoparticles dispersed in water. Hybrid nanofluids were prepared with varying volumetric ratios of 20:80, 40:60, 60:40, and 80:20 and examined across temperatures ranging from 15 to 45 °C. The influence of surfactants on stability was explored to augment thermal characteristics. Results revealed that the surfactants have a significant effect on stability and the specific mixing ratios can lead to more favourable thermal characteristics. Thermal conductivity enhancements, evaluated via the transient hot-wire method, demonstrated improvements of 7.43 %, 7.17 %, and 5.31 % for Ag/SiC (60:40), Ag/BeO (60:40), and SiC/BeO (80:20) hybrid nanofluids, respectively, compared to water. Viscosity measurements revealed Newtonian behaviour for the Ag, SiC, and BeO nanofluids, with a minimum viscosity enhancement of 3.01 % observed for the BeO nanofluid. Hybrid Ag/SiC nanofluid demonstrated a maximum viscosity enhancement of 4.90 % for 20:80 formulation. Density analysis showed maximum augmentation of 0.25 %, 0.097 %, and 0.0775 % for the Ag, SiC, and BeO nanofluids respectively at 0.025 vol% while hybrid Ag/SiC nanofluid exhibited a maximum of 0.23 % density increase for the 80:20 composition. The statistical models were also developed to predict properties against temperature. Furthermore, the cost analysis identified Ag nanofluid as the most expensive option, while the SiC/BeO hybrid was the most economical. However, the Ag-SiC (60:40) hybrid nanofluid offered a balanced trade-off between properties and cost.

1. Introduction

Nanofluids, with their exceptional thermophysical characteristics, offer a promising avenue to tackle energy-related challenges. Nanoparticles suspended fluids not only present new possibilities for harnessing, storing, and transferring energy but also hold the potential to significantly enhance the efficiency of heat transferring systems. This improved performance can play a pivotal role in mitigating pressing energy concerns, including issues like global warming, climate change, and the impending fuel crisis.

In 2007, Jana et al. [1] made a pioneering contribution to the field of nanofluid research by introducing hybrid nanofluids. Hybrid nanofluids are a groundbreaking innovation, as they comprise two different types of nanoparticles. These nanoparticles may belong to the same family in some cases, but more often, they come from distinct families. For instance, one type may be from the oxide family, which provides superior stability but lower thermal conductivity, while the other type is from the metallic family, offering superior thermal characteristics but lacking in stability. This characteristic allows hybrid nanofluids to harness the synergistic effects between these materials, resulting in significantly improved physical properties compared to traditional nanofluids. This approach has opened up exciting possibilities for enhancing various aspects of nanofluid performance. Hybrid nanofluids

* Corresponding authors.
E-mail addresses: h.babar@herts.ac.uk (H. Babar), h.wu6@herts.ac.uk (H. Wu).

https://doi.org/10.1016/j.molliq.2024.126175
Received 27 May 2024; Received in revised form 17 September 2024; Accepted 30 September 2024
Available online 2 October 2024

Nomenclature

Acronyms and Chemical Formulas

Ag	Silver
Al_2O_3	Aluminum Oxide
ANOVA	Analysis of Variance
BeO	Beryllium Oxide
CTAB	Cetyltrimethylammonium bromide
CNT's	Carbon nanotubes
CuO	Copper Oxide
DW	Distilled Water
d_p	Crystallite size
df	Degree of freedom
GA	Gum Arabic
GO	Graphene Oxide
HTC	Heat transfer coefficient
JCPDS	Joint Committee on Powder Diffraction Standards
k	Thermal conductivity [W/m °C]
MAE	Mean absolute error
MD	Molecular dynamics
MgO	Magnesium oxide
MWCNT's	Multi-walled carbon nanotubes
NIST	National Institute of Standards and Technology
PER	Performance Enhancement Ratio
PG	Propylene glycol
PRESS	Predicted Residual Error Sum of Squares
PVT	Photovoltaic-thermal
SDBS	Sodium dodecylbenzene sulfonate
SDS	Sodium dodecyl sulfate
SiC	Silicon Carbide
SiO_2	Silicon Dioxide/Silica
T	Temperature [°C]
TiO_2	Titanium Dioxide
TEM	Transmission Electron Microscopy
TPS	Transient Plane Source technique
WOS	Without surfactant
XRD	X-ray Diffraction
ZnO	Zinc Oxide

Greek Letter

ρ	Density [kg/m^3]
μ	Viscosity [kg/m.s]
λ	Wavelength of the X-rays
θ	Bragg angle

offer a versatile solution as they can be tailored to meet specific application requirements [2,3]. The ability to combine different nanoparticles allows for the optimisation of thermal properties while considering cost constraints. This adaptability makes hybrid nanofluids applicable across various industries and technological domains.

Khairul et al. [4] investigated the effects of Sodium Dodecylbenzene Sulfonate (SDBS, anionic) surfactant and particle concentration on several important properties of alumina-water and copper oxide–water nanofluids, including stability, viscosity, pH, and thermal conductivity. It was observed that increasing the concentration of nanoparticles could lead to an elevation in the pH levels of both nanofluids. This intriguing change is likely attributed to interactions occurring between the surface of nanoparticles and water molecules. Furthermore, the addition of SDBS surfactant had a similar effect, further pushing the pH towards the alkaline side. Their results revealed that an optimal surfactant concentration exists for each nanofluid formulation that maximises zeta potential magnitude, indicating stability. The optimised surfactant concentration also lowered viscosity and enhanced thermal conductivity. Ma et al. [5] examined the impact of various surfactants, i.e. Polyvinylpyrrolidone (PVP), Cetyltrimethylammonium bromide (CTAB), and Sodium dodecyl sulfate (SDS) on the stability and thermophysical properties of hybrid nanofluids of alumina (Al_2O_3), titania (TiO_2), and copper oxide (CuO). According to the results, the non-ionic surfactant PVP was found to be the most effective in retaining stability even at low concentrations. Interestingly, the viscosity values were found to remain close to water at lower PVP concentrations but increased significantly at higher concentrations due to excess surfactant molecules. Significant enhancements in thermal conductivity, with improvements of 12 % for Al_2O_3-CuO and 14 % for Al_2O_3-TiO_2 nanofluids, were achieved at 0.005 wt% and 0.01 wt% PVP concentrations, respectively. The results demonstrated the importance of surfactants in achieving stable nanofluids and improving their overall thermal characteristics. Kanti et al. [6] examined the thermophysical properties and stability of water-based graphene oxide (GO) and alumina and their hybrid nanofluids for solar energy applications. They used sol–gel and Hummer's methods for nanoparticle synthesis and assessed stability with different surfactants, finding PVP best for GO and SDBS for Al_2O_3 and hybrids. All the nanofluids demonstrated good stability even after 30 days. Ghadimi et al. [7] conducted a study to assess how the introduction of surfactants and the application of ultrasonication influence the stability and thermal characteristics of nanofluids consisting of titanium dioxide and water. The non-ionic surfactant SDS was found to reduce nanoparticle aggregation compared to preparations without surfactant, but only when coupled with ultrasonication. Ultrasonic horn processing for 15 mins and ultrasonic bath processing for 3 h both broke down agglomerations into smaller sizes. Analysis of absorbance measurements unveiled that nanofluids with SDS and ultrasonication had improved stability and dispersion compared to simple mixing. It is important to note that the viscosity of these nanofluids also exhibited an increase, likely attributed to the additional interactions between the nanoparticles, a phenomenon induced by the SDS surfactant and the ultrasonication process.

Li et al. [8] examined the influence of several control factors such as ultrasonic duration, temperature, and nanoparticle loading on the stability and viscosity of copper-ethylene glycol (Cu-EG) nanofluids. Copper nanoparticles (50 nm) were mixed with ethylene glycol at various mass fractions (1 %, 2 %, and 3.8 %), and subjected to ultrasonication for different durations in the rage of 15–75 mins. Viscosity measurements were carried out over a temperature range of 20 °C to 60 °C. The key findings indicated that viscosity decreased initially with increasing ultrasonication time, promoting better dispersion by breaking down larger nanoparticle clusters. Beyond an optimal time, further ultrasonication caused re-aggregation and increased viscosity. The optimal times were 60 mins for 1 % and 2 % mass fractions, and 45 mins for 3.8 %. Increasing temperature significantly decreased viscosity due to intensified Brownian motion, which disrupted clusters. A slight increase in mass fraction led to a marginal viscosity rise.

Guan et al. [9] explored the enhancement of thermal conductivity in hybrid nanofluids through molecular dynamics simulations, specifically focusing on Cu-Ag nanoparticles suspended in liquid argon (Ar). Their results showed that the Cu-Ag 50 %/Ar hybrid nanofluid outperforms unitary nanofluids, with a remarkable 69.7 % increase in thermal conductivity compared to pure liquid Ar. Analyses revealed that Ar atoms at the nanoparticle surface engage in dynamic equilibrium, influencing density, diffusion, and ultimately thermal conductivity. Their study also highlighted the potential of hybrid nanofluids for optimising heat transfer by fine-tuning nanoparticle material combinations and ratios to enhance the nanolayer structure and dynamics. Contreras et al. [10] investigated the thermohydraulic characteristics of graphene and silver nanofluids as automotive coolants. The nanofluids were formulated by dispersing nanoparticles within a mixture of water and ethylene glycol

in a 50:50 ratio. To evaluate practical performance, heat transfer experiments were carried out within an automotive radiator test configuration. The results revealed that, in comparison to the base fluid, thermal conductivity of nanofluids exhibited enhancements ranging from 1.3 % to 9.2 % for silver and 2.4 % to 9.2 % for graphene. The viscosity was found to be increased by 10.8 % for silver in comparison to the base fluid, however, a noticeable decrease was observed as the temperature rose. Additionally, the findings demonstrated that silver nanofluids illustrated a notable maximum heat transfer enhancement of 4.7 %, suggesting their potential to enhance the performance of automotive cooling systems. However, it was observed that graphene nanofluids yielded varying outcomes, indicating limited benefits in this particular application. Sharma et al. [11] investigated the thermophysical properties of polydisperse SiO_2 nanoparticles dispersed in an aqueous glycerol mixture. The nanofluids were formulated with different sizes of nanoparticles (15, 50, and 100 nm) in a glycerol-water mixture at concentrations of 0.5 vol% and 1.0 vol%. The results demonstrated a clear trend of increasing thermal conductivity with rising temperature for both the base liquid and the nanofluids. At 0.5 vol % and 60 °C, SiO_2 concentration, the thermal conductivity exhibited an increase of 11.1 % relative to the base liquid while the addition of nanoparticles led to a 32 % rise in viscosity. Kanti et al. [12] investigated graphene oxide (GO)-based hybrid nanofluids for thermal applications. The hybrid formulations of graphene oxide, silica, and titania were prepared with a 50:50 ratio, varying particle concentrations from 0.05 vol% to 1 vol%. The study examined viscosity and thermal conductivity between 30 °C and 60 °C and used the Performance Enhancement Ratio (PER), which is the ratio of thermal conductivity enhancement to viscosity enhancement, to rate their overall performance. It was observed that the pure GO nanofluids showed the highest thermal conductivity enhancement, 9.8 % more than GO-TiO_2 and 14.4 % more than GO-SiO_2 at 60 °C and 1.0 % volume concentration. However, pure GO also exhibited the greatest viscosity enhancement compared to the hybrid formulations. The PER analysis suggested that hybrid nanofluids are promising for high-temperature, cost-effective thermal applications above 45 °C.

Esfe et al. [13] conducted an experimental study on the thermophysical properties and heat transfer characteristics of Ag-water nanofluids in turbulent flow through a straight tube. They investigated the impact of silver nanoparticle volume concentration (up to 1 %) on thermal conductivity, dynamic viscosity, convective heat transfer, and pressure drop. The thermal conductivity of the nanofluid samples was measured experimentally using a KD2 Pro thermal property analyser, while the dynamic viscosity was determined using a Brookfield viscometer. The authors utilised mixing theory to calculate nanofluid density and the thermal equilibrium model to compute specific heat capacity [14,15]. Experimental thermal conductivity data were compared with various models reported in the literature, which were found to underestimate the calculated values. Additionally, a new correlation was proposed for dynamic viscosity of Ag-water nanofluids based on their findings. The results showed that increasing the nanoparticle concentration and Reynolds number led to an enhancement in the Nusselt number. At a volume concentration of 1 % and a Reynolds number of approximately 22,000, the Nusselt number increased by 11.8 %. However, the pressure drop also increased by an average of 15.75 % with 1 % volume concentration. The authors evaluated the thermal performance factor, finding that the heat transfer enhancement outweighed the pressure drop penalty for the range of concentrations studied, with a maximum thermal performance factor of 1.18 at 1 % volume concentration. Chen et al. [16] developed a spiral microreactor for continuous, high-throughput synthesis of stable silica (SiO_2) nanofluids with precisely controlled particle size. The synthesized nanofluids were utilised for flow boiling heat transfer experiments, demonstrating significant enhancements in both critical heat flux (up to 124 %) and heat transfer coefficient (up to 153 %) on a micro pin-fins silicon chip surface at extremely low pressure drop. Maddah et al. [17] studied the effect of silver and alumina nanoparticles on the thermophysical properties of nanofluids. The samples were prepared by dispersing Ag and Al_2O_3 nanoparticles with nominal diameters of 40 nm and 20 nm respectively in distilled water at various volume concentrations ranging from 0.25 % to 5 %. Thermal conductivity and viscosity of the nanofluids were measured at 15 °C using a KD2 analyser and Brookfield viscometer. According to the results, the thermal conductivity, electrical conductivity, and viscosity of the nanofluids increased with increasing nanoparticle volume fraction. The thermal conductivity and electrical conductivity increased linearly, while the viscosity showed a nonlinear increase at volume fractions above 2 %. The nanofluids exhibited Newtonian behaviour at lower concentrations (0.25 % to 2 %) but transformed to non-Newtonian fluids at higher concentrations. It is concluded that although high thermal conductivity is desirable for heat transfer applications, the concurrent rise in viscosity is a crucial factor to consider for fluid flow.

Huminic et al. [18] studied the thermophysical properties of water-based nanofluids containing silicon SiC nanoparticles for heat transfer applications. They synthesized SiC nanoparticles via laser pyrolysis and prepared stable nanofluids with concentrations of 0.5 and 1.0 wt% using a carboxymethylcellulose surfactant. Their results revealed that increasing the surfactant concentration decreased the thermal conductivity but raised the viscosity and surface tension of the base fluid. Additionally, the study assessed the heat transfer performance of a two-phase closed thermosyphon utilising the SiC nanofluids as working fluids. These nanofluids demonstrated improved heat transfer rates of up to 24.4 % for 1.0 wt%, along with enhanced evaporator heat transfer coefficients and reduced thermal resistance by up to 32.8 % compared to water, with better performance observed at higher nanoparticle concentrations. Luo et al. [19] prepared oil-based SiC nanofluids with a wide concentration ranged 0.1–10.3 vol% using the two-step method for immersion cooling applications in data centres. The thermal conductivity exhibited a maximum enhancement of 25.5 % for 10.3 vol% nanofluids at 30 °C, while the specific heat capacity decreased by up to 22.5 % compared to the base mineral oil. Additionally, viscosity showed a moderate increase, with a maximum increment of 35 % for the 10.3 vol % nanofluids. Through numerical simulations and experiments, they identified the optimal nanofluid concentrations for different Reynolds numbers. At low Reynolds numbers ($\leq$1000), nanofluids with 0.3 and 0.5 vol% concentration showed better heat transfer performance, with a maximum enhancement of 11.4 % for the 0.3 vol% nanofluids at Re = 250. At higher Reynolds numbers (>1000), nanofluids with 3.7 vol% concentration performed better, achieving a maximum enhancement of 11.7 % at Re = 500, due to their enhanced thermal conductivity. They stated that lower concentrations are preferable for applications where the fluid rate is lower, or the Reynolds number is under 1000. Sheikholeslami and Khalili [20] explored the solar photovoltaic-thermal (PVT) system using eco-friendly graphene nanoplatelets (graphene nanoplatelets (GNP) nanofluid to enhance heat transfer. They employed an eight-lobed tube with copper fins and tested GNP at 0.025 % and 0.1 % weight fractions. The system achieved maximum exergy and thermal efficiencies of 15.32 % and 55.22 % respectively, using 0.1 % GNP at a Reynolds number of 1611. The GNP nanofluid improved cooling, boosting electrical efficiency by 5.8 %, and increased CO_2 reduction by 7.1 tons compared to water, highlighting its environmental benefits. In another study, Sheikholeslami et al. [21] investigated the PVT system featuring a cylindrical reflector, a thermoelectric generator (TEG) made from Cu_2SnS_3 (CTS), and a MgO-water nanofluid spectral filter. The nanofluid improved cooling, enhancing system performance by 36.3 %. The combined system doubled CO_2 reduction compared to conventional PV systems, showing strong energy efficiency and environmental benefits. These studies demonstrated that incorporating nanofluids into various systems can significantly reduce carbon dioxide emissions. This reduction is achieved by enhancing the overall performance and efficiency of these systems. By optimizing the performance of systems such as cooling and heating mechanisms, nanofluids contribute to a greener,

more sustainable approach to energy consumption.

Abbasi et al. [22] employed molecular dynamics (MD) simulations to investigate the effects of particle shape and base fluid type on the density of nanofluids. They considered the ternary mixture formula, which accounts for the formation of a nanolayer around the nanoparticles, to predict the nanofluid density more accurately. Two base fluids, water and liquid argon, were examined along with four different nanoparticle shapes: spherical, planar, block, and rod-shaped with varying aspect ratios. The results revealed that the thickness of the nanolayer was influenced by the base fluid type, with liquid argon forming a slightly thicker nanolayer (1.3 nm) compared to water (0.9 nm). Additionally, the density of the nanolayer was found to be higher for planar nanoparticles than for spherical and rod-shaped particles. Additionally, the density of the nanolayer was found to be higher for planar nanoparticles than for spherical and rod-shaped particles. This was attributed to the flat surfaces of planar particles being more effective in absorbing base fluid molecules to form the nanolayer. Furthermore, the density of nanofluids containing planar or spherical nanoparticles decreased with increasing particle diameter. Shoghl et al. [23] conducted a series of experiments to analyse the thermophysical properties of six different water-based nanofluids: CuO, TiO_2, MgO, MWCNT, Al_2O_3, and ZnO. They examined the density, viscosity, and electrical conductivity of these nanofluids as functions of nanoparticle concentration and temperature. The findings showed a considerable enhancement in electrical conductivity and viscosity of the base fluid upon the addition of nanoparticles, while the density showed a moderate increase. According to the results, a linear trend was observed between electrical conductivity and nanofluid concentration for all nanofluids except MWCNT, which exhibited a percolation threshold at 0.1 wt%. The sample containing ZnO nanoparticles exhibited highest conductivity at lower concentrations, while CNT nanofluids showed peak values at higher concentrations. The study also concluded that the density values could be accurately predicted by the mixture rule, and the viscosity data agreed well with the Einstein model at low concentrations but deviated at higher concentrations, which was attributed to nanoparticle agglomeration. However, the Maxwell model failed to predict the enhancement in electrical conductivity, leading the researchers to develop correlations for each nanofluid type based on the experimental data. A study conducted by Sitti et al. [24] examined the effect of temperature, volumetric concentration, and nanoparticle size on the density variation of various nanofluid samples. They measured the densities of nanofluids containing nanoparticles of Al_2O_3, ZnO, CuO, TiO_2, SiO_2, and CNTs dispersed in a base fluid of 60:40 propylene glycol and water (PG/W) by volume. The measurements were carried out over a temperature range of 0–90 °C and with nanoparticle volumetric concentrations up to 6 %. The experimental results were compared with the theoretical equation proposed by Pak and Cho, which relates the nanofluid density to the densities of the base fluid and nanoparticles, as well as the nanoparticle volumetric concentration. It was found that the measured densities agreed well with the theoretical predictions, with a maximum deviation of 3.8 % observed for the copper oxide nanofluid. The average deviation between the experimental data and the theoretical equation was only 0.1 % for all 874 data points.

The analysis of the Scopus database data presents a critical perspective on the state of research in the field of nanofluids and their hybrid combinations. The data reveals a growing interest in nanofluid research, as evident from the steady increase in the number of published articles, especially from 2005 onwards, as shown in Fig. 1. The stats indicate that nanofluids are an active and dynamic area of study. While there is substantial research on “Nanofluid” alone, the data illustrates that the hybrid nanofluid combinations (Ag-SiC, Ag-BeO, and SiC-BeO) have received considerably less attention throughout the years. This scarcity of research on these hybrid nanofluids emphasises the novelty of our study. The lower publication counts for the hybrid nanofluid combinations suggest that there is ample room for original research and contributions in this area. The study can address this gap and potentially lead to groundbreaking findings, further enhancing the understanding and applications of hybrid nanofluids. According to the bibliometric analysis, silver nanofluids have witnessed a period of steady growth in publications from 2005 to around 2014, suggesting a relatively established area of research. SiC nanofluids have displayed a consistently low and stagnant publication output, with only a slight increase in recent years, indicating an underexplored composition. BeO nanofluids, a newer addition to the literature starting around 2019, have seen limited attention, emphasising their underexplored nature.

The choice of nanoparticles for this study is based on a thorough

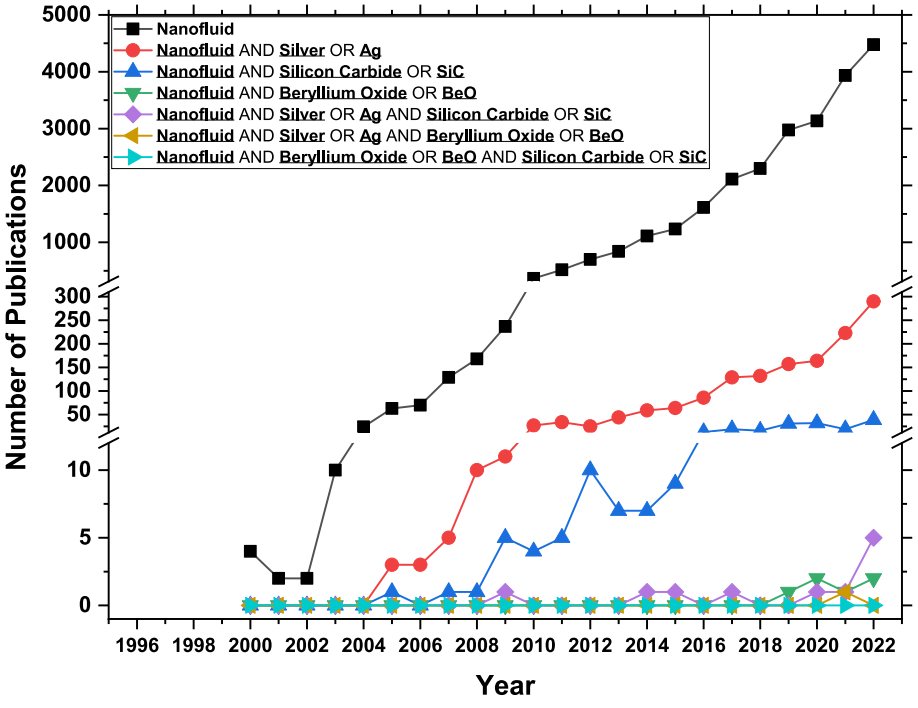

Fig. 1. Publication trends on nanofluids and hybrid nanofluid combinations based on Scopus database.

consideration of their thermal properties, cost, and density. Silver nanoparticle was selected from the metal family due to its high thermal conductivity. However, its higher density poses challenges for maintaining long-term suspension in base fluids like water, while its elevated cost hinders practical implementation. In contrast, SiC and BeO nanoparticles were chosen from the carbide and oxide families, respectively, due to their lower cost and density. Despite these benefits, SiC and BeO have different properties that can be advantageous for specific applications. SiC may enhance thermal properties, making it suitable for applications in aerospace and automotive cooling, while BeO offers excellent electrical insulation, making it valuable for electronic cooling and nuclear applications. Hybrid nanofluids such as Ag-SiC are particularly effective for high-performance cooling systems used in aerospace and automotive applications, as well as for precision machining processes due to their enhanced thermal properties. In contrast, Ag-BeO nanofluids capitalize on silver's thermal conductivity combined with BeO's electrical insulation, making them well-suited for electronic cooling systems, high-power laser applications, and nuclear reactors. Meanwhile, SiC-BeO nanofluids, are ideal for advanced energy storage systems, nuclear reactors, and high-temperature industrial processes. The potential synergistic effects of combining Ag-SiC, Ag-BeO, and SiC-BeO remain largely unexplored, highlighting the novelty and potential of these hybrid nanofluids. The limited prior research indicates significant opportunities for innovative discoveries and applications in these areas. Focusing future research efforts on these nanofluid combinations could provide new insights compared to the more established singular nanofluid types like silver or silicon carbide alone. The data-driven approach here demonstrates the value of conducting thorough background reviews and analyses to identify promising new research directions. As technology and industrial applications continue to advance, the development of new nanofluid combinations with unique properties will be in high demand.

This study aims to conduct a comprehensive examination of the thermophysical properties of these hybrid nanofluids. The investigation will encompass a wide spectrum of temperatures and involve varying mixing ratios. By doing so, this research seeks to address a notable lacuna in the existing scientific literature, thereby contributing substantively to the understanding of these unique nanofluid compositions. The outcomes of this research endeavour are anticipated to serve as a valuable resource with practical implications across a multitude of scientific and engineering applications, thereby advancing the field's knowledge base and utility.

2. Preparation of nanofluid

Numerous researchers have adopted the two-step method for preparing nanofluids, recognized as an efficient and cost-effective approach for generating substantial solution volumes. This study is structured into three distinct segments: The initial phase investigates the impact of diverse surfactants on samples of silver, beryllium oxide, and silicon carbide, each prepared at a particle loading of 0.01 vol%. In the subsequent phase, various fluids are prepared by altering particle

Table 1
Properties of the particles.

Nanoparticle	Formula	Size	Purity	Thermal Conductivity (W/m.K)	Density (g/cm^3)	Quantity (g)	Cost (£)*	Reference
Silver	Ag	10–40 nm	99.9 %	429	10.5	25	655	[25]
Silicon carbide – (beta-phase)	SiC	45–55 nm		360	3.15	25	143	[26]
Beryllium oxide	BeO	85–140 nm	99 %	285	3.01	25	131	[27,28]

*Prices as of February 1st, 2024.

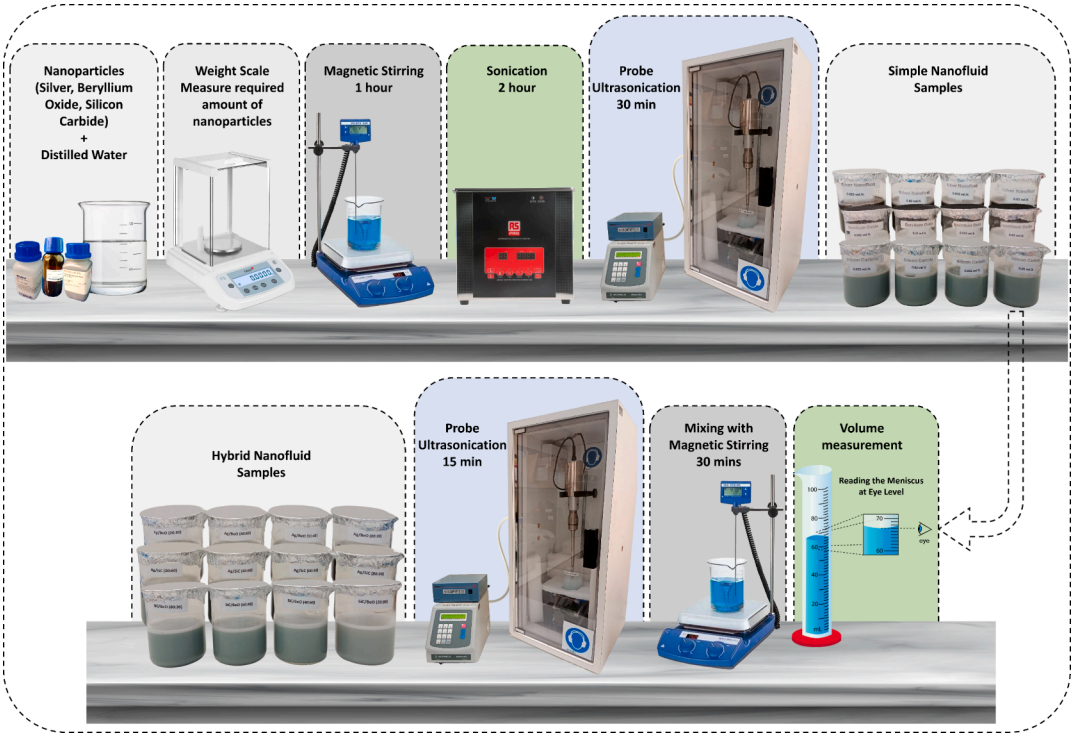

Fig. 2. Schematic representation of the nanofluid preparation method.

concentrations within the range of 0.01 vol% to 0.025 vol%, aiming to assess stability and determine optimal concentrations for hybrid samples. The final segment encompasses the formulation of hybrid nanofluid samples (Ag/BeO, SiC/BeO, and Ag/SiC) at different mixing ratios, specifically examining the thermophysical properties across varying temperatures ranging from 15 − 45 °C. The nanoparticles utilised in this study were procured from Alfa Aesar and Thermo Fisher Scientific, two well-known suppliers in the field. Table 1 provides the properties of the nanoparticles including the details of the size, purity, thermal conductivity, density, and cost. All samples undergo a series of processes involving magnetic stirring, ultrasonication in a sonication bath, and final treatment with high-wave ultrasonication using a sonication probe.

To make unitary nanofluids, the following steps are followed: the calculated amount of nanoparticles is added to the desired quantity of base fluid while stirring for 1 h. Subsequently, bath sonication and probe ultrasonication of the fluid are carried out for 2 h and 30 mins, respectively, utilising an RS Pro ultrasonicator and NanoSight probe sonicator. These sonication processes are essential for breaking down agglomerated nanoparticles into individual particles, ensuring uniform suspension. Finally, to formulate the hybrid nanofluids having different mixture ratios, each nanofluid is prepared separately with the desired particle concentration and then mixed accordingly while carrying out continuous stirring with the help of a magnetic stirrer. To ensure the proper mixing of fluids, the processed solution will be further sonicated with the help of probe sonication for 15 mins. Fig. 2 illustrates the schematic representation of the steps involved in the preparation of hybrid nanofluids.

3. Effect of surfactant on stability and pH value

A widely employed strategy for enhancing the stability of nanofluids involves the incorporation of surfactants, a class of compounds renowned for their ability to engender electrostatic or steric repulsion forces among nanoparticles. This judicious utilisation of surfactants serves as an effective means to prevent the undesired agglomeration of these minute particles, thereby bolstering the enduring stability of nanofluid systems. A study was carried out to delve into how different surfactants impact the overall stability of nanofluids, as well as their influence on the pH levels upon surfactant introduction. This investigation aims to shed light on the intricate interplay between surfactants and nanofluid stability while simultaneously observing their ramifications on pH values. The resulting repulsive interactions among nanoparticles not only thwart their agglomeration tendencies but also contribute to the preservation of the desired dispersion, ensuring the continued, homogeneous distribution of nanoparticles within the fluid medium.

The Hanna pH meter (HI 98128) used in this study has an accuracy of ± 0.05 pH, ensuring precise pH measurements. While the meter came with a calibration certificate, an additional calibration step was performed to ensure the utmost accuracy in the pH measurements. The calibration procedure utilised a specific method involving two buffer solutions provided with the instrument, having pH values of 4.01 and 7.01.

To commence the calibration process, the tailing side of the pH meter was immersed in a cleaning solution, which effectively cleaned the temperature sensor and pH electrode. Subsequently, the meter was set to the calibration mode, and it was first submerged into the buffer solution with a pH of 4.01. The meter recorded the corresponding pH reading. After cleaning the sensor and electrode again, the meter was immersed in the second buffer solution, and its pH value was recorded. Following the completion of the calibration process, the pH of a neutral solution was measured to verify the accuracy of the meter's readings. This thorough calibration procedure ensured the reliability of the pH measurements throughout the study. The fluid preparations were conducted in an open environment, exposing the distilled water to atmospheric air. In such conditions, the pH range of the distilled water utilised could vary from 5.4 to 5.7 [29]. As observed in this study, the pH value of the base fluid was noted to be 5.67 ± 0.02.

The stability of nanofluid suspensions is paramount, and the addition of surfactants has been widely acknowledged for their role in stabilising nanoparticles, impeding agglomeration, and altering surface characteristics. Silver, beryllium oxide, and silicon carbide nanofluids were prepared both without surfactants and with the addition of CTAB, SDS, Gum Arabic, and SDBS. The pH values were measured using a calibrated pH meter at 20 °C. Each measurement was repeated thrice to ensure accuracy and reliability. It was noticed that the addition of Ag and BeO nanoparticles made the nanofluid slightly basic compared to distilled water, while the SiC nanoparticles had an acidic effect.

For this study, samples were formulated with a particle volume fraction of 0.01 % vol. This study employed a preparation method that involved 1 h of magnetic stirring, followed by 1 h of sonication in a sonication bath, and ultimately 15 mins of sonication using an ultrasonication probe to produce the samples. During the sample preparation, an equivalent amount of surfactant, matching the quantity of particles, was introduced into the solution. The solutions were maintained at room temperature and monitored throughout the observation period.

The nanofluid samples were observed over 7 days to evaluate their long-term stability with the addition of different surfactants. The stability observation of nanofluids with different surfactants is depicted in Fig. 3. It was found that the solutions containing the anionic surfactant SDBS showed the best stability overall for the three nanoparticle types tested. The SDBS-containing nanofluids maintained their dispersion with minimal sedimentation and aggregation over the 7-day period. This indicates that SDBS provided excellent electrostatic and steric stabilization for the suspended nanoparticles. For the beryllium oxide nanofluids specifically, the addition of the anionic surfactant SDS was found to have the worst effect on stability. The silicon carbide nanofluid with SDS had even poorer stability than the surfactant-free sample, with significant sedimentation and aggregation occurring within days. This suggests SDS interacted poorly with the silicon carbide surface, neutralizing surface charge and inducing rapid particle aggregation. After SDBS, the cationic surfactant CTAB provided the next best stability enhancement for the nanofluids. The CTAB-containing samples showed good dispersion stability over the 7 days, with only minor sedimentation in some cases. The positively charged CTAB likely electrostatically stabilized the nanoparticles.

The pH values exhibited distinctive variations in nanofluid samples treated with different surfactants compared to the surfactant-free nanofluids and the reference distilled water, as shown in Fig. 4. The silver nanofluid experienced a shift towards both higher and lower pH values, contingent upon the type of surfactant introduced. Similar trends were observed in the beryllium oxide and silicon carbide nanofluids, indicating diverse responses to distinct surfactants.

For the silver nanofluid without surfactant, the measured pH was 6.24. The addition of the cationic surfactant CTAB caused a small decrease in pH to 6.1. This suggests that CTAB interacted with the silver nanoparticles, partially neutralizing the surface charge. The anionic surfactants SDS and GA also decreased the silver nanofluid pH, to 5.85 and 5.58 respectively. Interestingly, SDBS induced a considerable increase in pH from 6.24 to 7.2, indicating a more alkaline nature.

For the beryllium oxide nanofluid, the pH decreased from 5.95 to 5.57 upon the addition of CTAB. The inclusion of SDS resulted in a pH drop to 5.53, whereas Gum Arabic led to a slight increase in pH to 5.85. As anticipated, the SDBS demonstrated a significant pH increase, elevating the pH to 7.08. The surfactants affect the pH value of Silicon carbide nanofluid in a different way as the suspension of particles made the solution more acidic and noticed a pH value of 5.56. The supplementation of CTAB surfactant showed a slight increase in this value to 5.76 while SDS made the solution more acidic with a minor decrease in pH value to 5.31. Additionally, Gum Arabic resulted in a pH elevation of 6.1, while SDBS significantly increased the pH to 7.45.

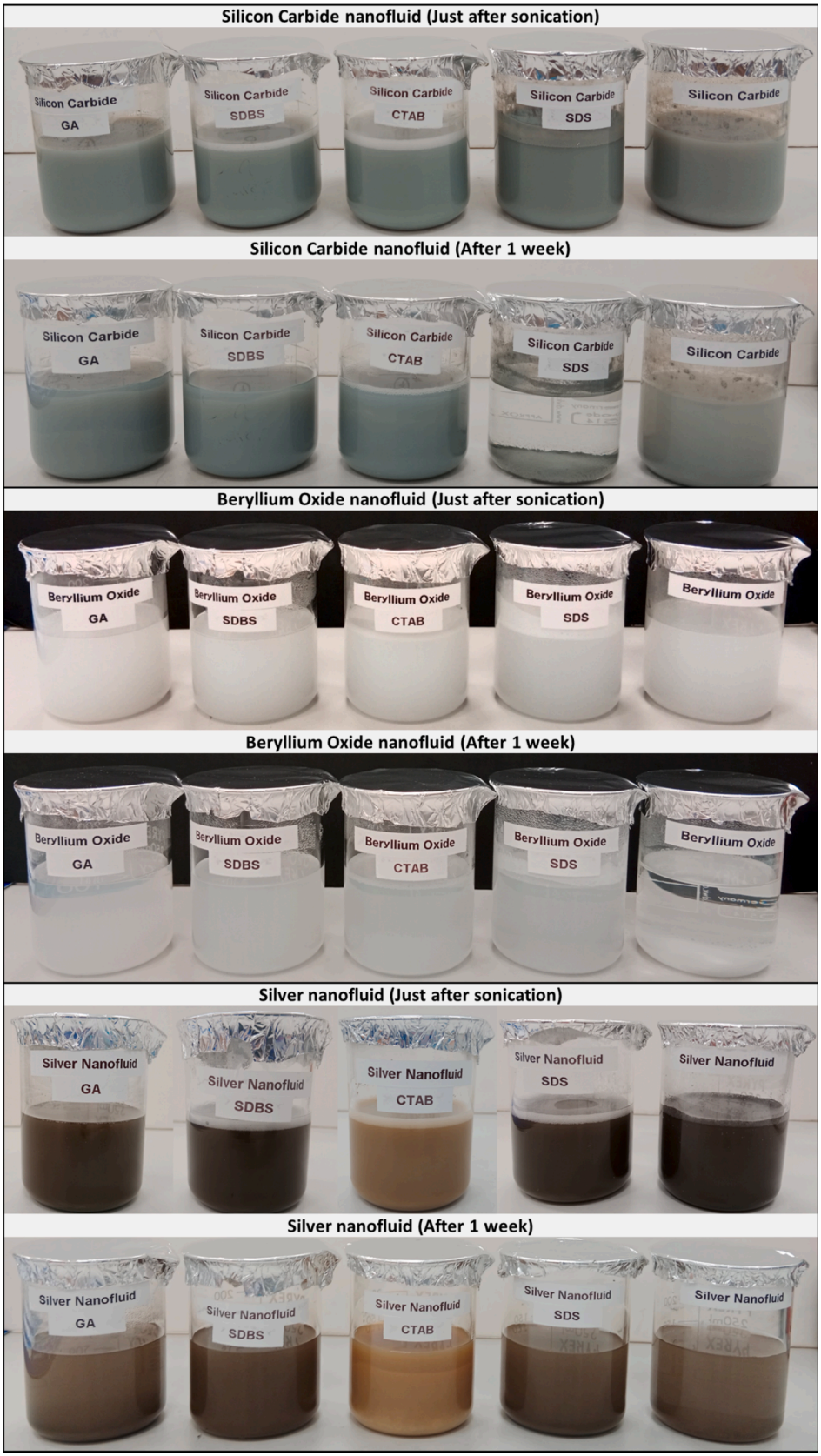

Fig. 3. Stability observation of nanofluids with different surfactants.

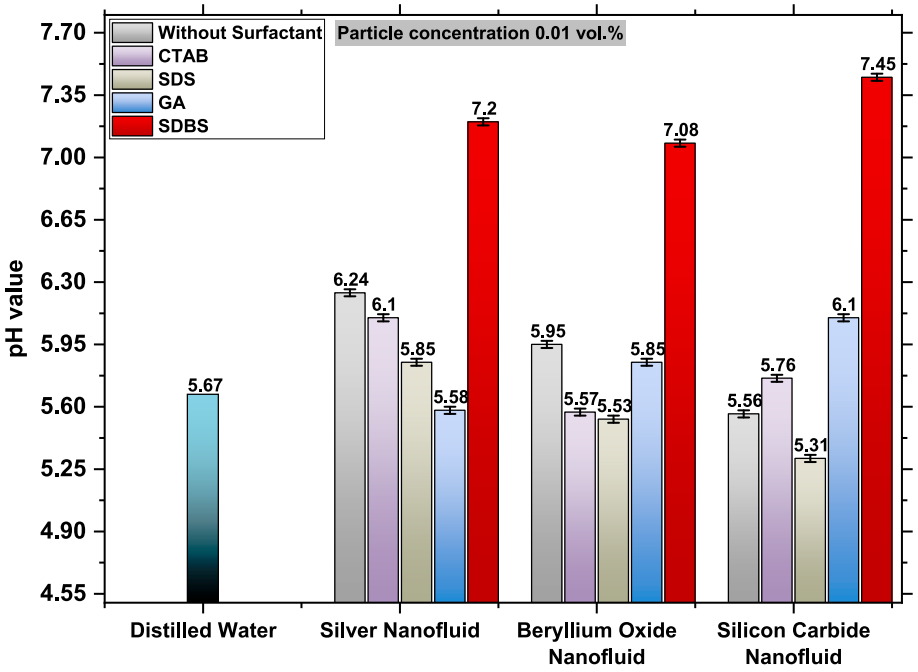

Fig. 4. Ph values of nanofluids with different surfactants.

Notably, the SDBS surfactant consistently induced a substantial rise in pH across all three types of nanofluids, significantly shifting the values toward neutrality. The addition of CTAB and GA to the nanofluids had a mixed effect on the pH. The addition of these surfactants decreased the pH of silver nanofluid and beryllium oxide but increased the pH of silicon carbide nanofluid.

The effect of SDBS on the pH of nanofluids is more complex. SDBS is an anionic surfactant, but it can also form micelles in aqueous solution [30]. Micelles are aggregates of surfactant molecules that have a hydrophilic outer layer and a hydrophobic inner core. When SDBS is added to a nanofluid, it can form micelles around the nanoparticles. The micelles can trap the nanoparticles inside and prevent them from interacting with the water molecules. This can lead to an increase in the pH of the nanofluid. While the pH approximation to neutral by SDBS indicates potential stability, it is crucial to conduct further analysis to comprehend the precise mechanisms by which SDBS interacts with nanoparticles, stabilising the nanofluids. Such investigations can validate the observed pH effects and solidify the link between near-neutral pH and enhanced stability, offering insights for practical applications in various fields where stable nanofluids are indispensable.

Fig. 5 showcases pH values of different nanofluids containing varying concentrations of nanoparticles, all prepared using SDBS surfactant in which the quantity of surfactant added in the solution is equal to the particles' weight. It displays the pH values corresponding to different

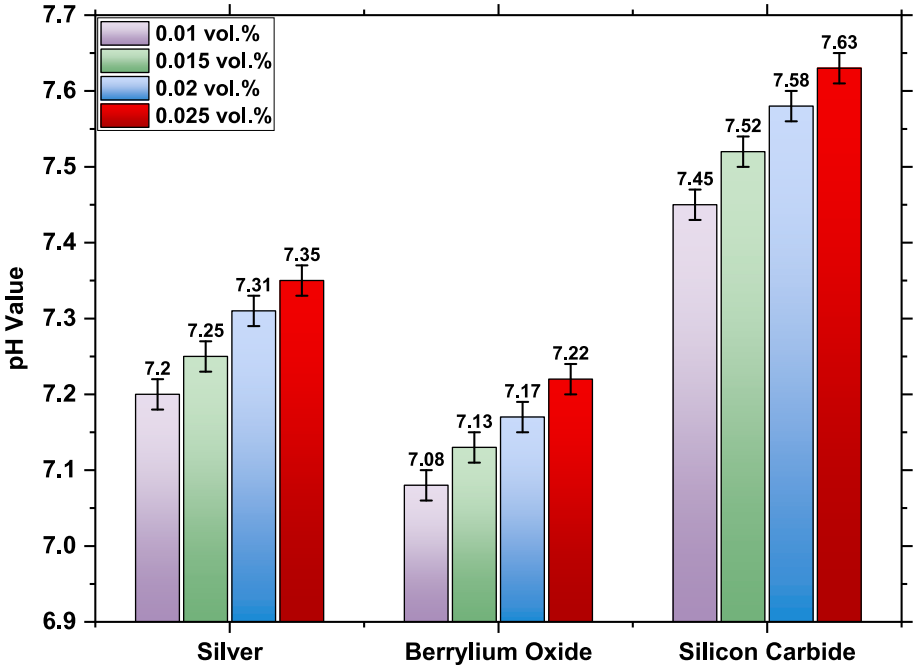

Fig. 5. Ph values of nanofluids with varying particle concentrations (0.01——0.025 vol%) using SDBS surfactant.

particle concentrations of Ag, BeO, and SiC at 0.01, 0.015, 0.02, and 0.025 vol%. According to the results, a noticeable elevation in the pH values for all types of nanofluids investigated was observed as the concentration of particles and relatively the amount of surfactant increased. Silver nanoparticles exhibited a relatively moderate increase in pH as the concentration raised from 0.01 to 0.025 vol%, with a change from 7.2 to 7.35, however, beryllium oxide and silicon carbide displayed more pronounced shifts in pH values. The results revealed that the BeO nanofluid experienced a more significant increase in pH, from 7.08 to 7.22, across the same concentration range, while the SiC solution showed an even more substantial shift, moving from 7.45 to 7.63.

This variation in the rate of pH change could be attributed to several factors specific to each type of nanoparticle. One influential factor could be the inherent chemical properties of the nanoparticles themselves. For instance, differences in surface charge, composition, or reactivity of the nanoparticles could lead to varied interactions within the solution, influencing the solution's pH differently. Importantly the interaction of these nanoparticles with the SDBS surfactant might not be uniform across all types. The diverse chemical affinities or reactions between nanoparticles and the surfactant may result in differing effects on pH, contributing to the observed variations. Furthermore, factors such as nanoparticle size, shape, and concentration could also significantly contribute to this variability. Distinct physical properties of different nanoparticles could impact pH alterations differently. Smaller particles, in some cases, exert a more noticeable influence on solution pH compared to larger particles at similar concentrations.

The objective behind formulating nanofluids at different concentrations was to determine the most suitable concentration for the synthesis of hybrid nanofluids, focusing on their stability. All the suspensions were kept under observation over the course of a week, and it was observed that nanofluid samples containing Ag and BeO nanoparticles at a concentration of 0.025 vol% began exhibiting nanoparticle settling after four days, resulting in the formation of a clear upper layer. In contrast, the SiC suspension remained stable during the observation period, as depicted in Fig. 6.

A study was also carried out to observe the pH value of various hybrid nanofluids prepared by mixing different ratios of individual nanofluids at a concentration of 0.025 vol%, as depicted in Fig. 6. The study aimed to examine how these mixtures' pH values changed with varying proportions of the constituent nanofluids. The observed pH values of the hybrid nanofluids indicated intriguing trends across the different mixing ratios, as presented in Fig. 7. The results revealed that the pH variations were not uniform across all hybrid combinations, suggesting specific interactions between the nanoparticles at different ratios. As anticipated, for the Ag/BeO hybrid nanofluid, an increase in the Ag concentration led to a gradual rise in pH, culminating in the highest pH value of 7.33 at the 80/20 ratio. This shift in pH can be attributed to the inherently higher pH value of Ag in comparison to BeO. Moreover, the SiC/BeO hybrid nanofluid showcased a consistent

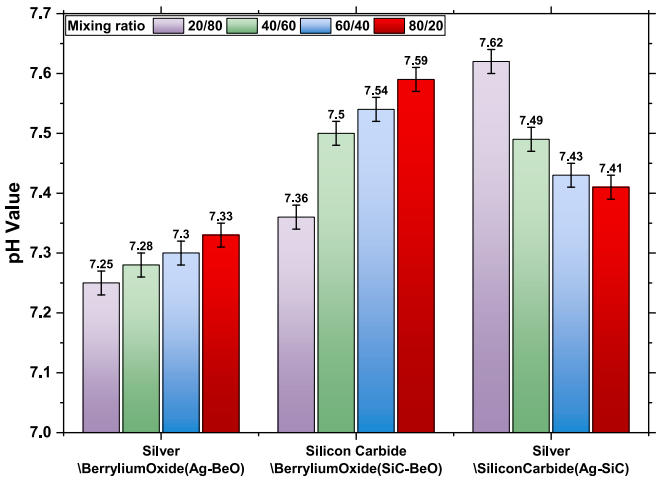

Fig. 7. Ph values of hybrid nanofluids (ag/beo, sic/beo, and ag/sic) with different mixing ratios (20/80, 40/60, 60/40, and 80/20).

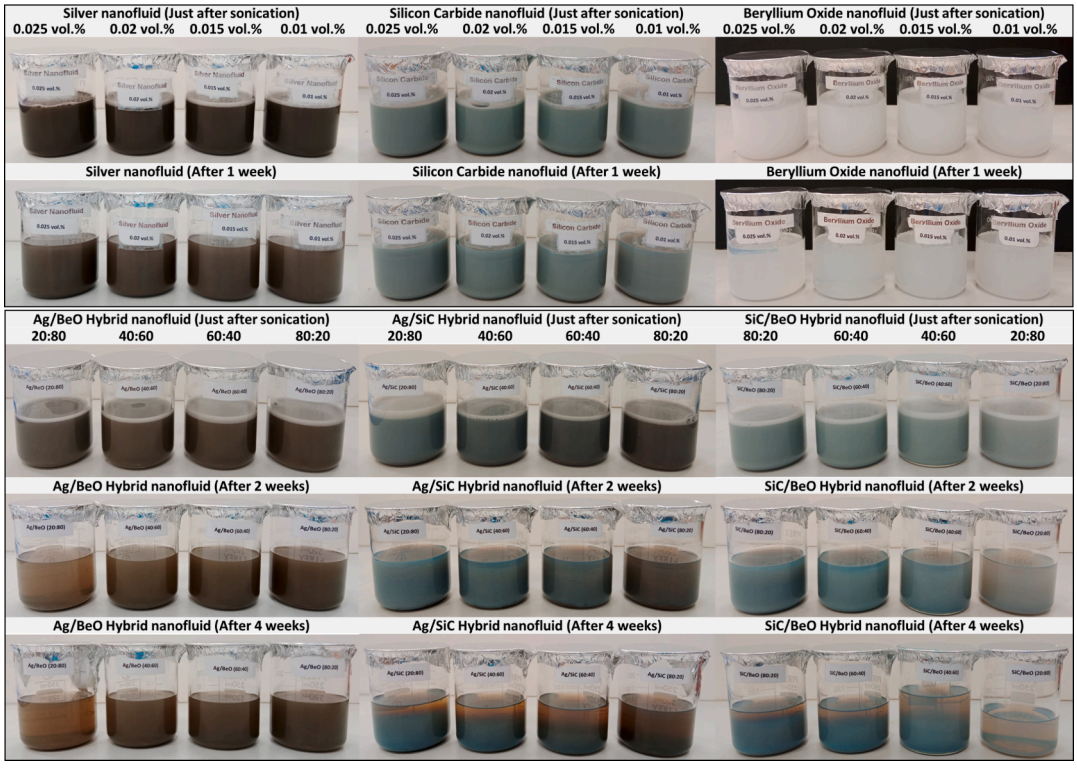

Fig. 6. Stability observation of simple and hybrid nanofluids over time.

escalation in pH as the proportion of SiC increased. The pH values increased steadily, reaching a maximum of 7.59 at the 80/20 ratio, reflecting the notably higher pH value of the SiC solution compared to Ag. Finally, as the pH value of SiC solution was significantly higher than Ag, the hybrid nanofluid of Ag/SiC exhibited a decrease in pH values with an increase in the proportion of Ag.

Understanding pH variations is crucial for tailoring nanofluids for diverse applications. Controlling and predicting pH changes of hybrid nanofluids could aid in optimising their stability and functionality in specific technological or industrial applications, such as heat transfer systems or biomedical uses.

4. Characterisation

The comprehensive characterisation of nanoparticles and nanofluid dispersion involved a multifaceted approach, combining X-ray Diffraction (XRD) and Transmission Electron Microscopy (TEM) analyses to elucidate the structural properties of the nanoparticles. Additionally, the nanofluid stability and particle size distribution were meticulously examined using a Malvern Zetasizer, providing a holistic understanding of their physicochemical behaviour.

4.1. X-ray diffraction (XRD)

X-ray diffraction (XRD) is utilised to analyse the crystallographic structure, crystallite size, and phase composition of silver, beryllium oxide, and silicon carbide nanoparticles, revealing intricate details about their atomic arrangements. X-ray diffraction tests have been reported in numerous research studies for the characterisation of nanoparticles as well as various pure or composite materials [31,32]. The analysis was carried out utilising an X-ray diffractometer (Bruker – D8 Advance) with Cu-Kα radiation (wavelength: 1.5406 Å, energy: 8.05 keV). In the case of silver nanoparticles, four distinct peaks were identified at 2θ angles of approximately 38.12°, 44.30°, 64.45°, and 77.4°, as shown in Fig. 8(a). The XRD curve pattern and the positions of the peaks aligned with the previously reported literature data on silver [33,34]. These peaks were indexed to the (111), (200), (220), and (311) planes of a face-centred cubic (FCC) silver crystal structure. The lattice parameter was determined as a = 4.089 Å, with a corresponding unit cell volume of V = 68.39 Å^3. The findings also concurred with the reported data of the Joint Committee on Powder Diffraction Standards JCPDS data (JCPDS 04–0783) for silver nanoparticles. Moreover, the most prominent peak in the spectrum suggests that the nanoparticles exhibit a preferred orientation, with their (1 1 1) planes aligned parallel to the surface. Fig. 8(b) shows the intensity of X-rays diffracted by a sample of beryllium oxide nanoparticles as a function of the 2θ angle.

The curve peaks indexed to the α-BeO phase, which is the most stable form of beryllium oxide at room temperature. The peaks observed at crystalline angles of 38.40°, 41.06°, 43.76°, 57.47°, 69.44°, and 76.70° correspond to the (100), (002), (101), (102), (210), and (103) reflections of α-BeO, respectively, as predicted by the JCPDS file for this material (JCPDS 35–0818). Additionally, the curve confirmed the presence of hexagonal wurtzite beryllium oxide nanoparticles with a random orientation. The lattice parameters for BeO nanoparticles were found to be a = 2.705 Å and c = 4.39 Å, yielding a unit cell volume of V = 27.84 Å^3. Wang et al. [35] examined the characteristics of BeO nanoparticles at different temperature values and identified a consistent X-ray diffraction (XRD) curve pattern. Additionally, they observed an increase in the intensity of peaks with rising temperatures. The XRD curve of the silicon carbide nanoparticle has been shown in Fig. 8(c). The number of sharp peaks indicated that the studied nanoparticles are highly crystalline and have a cubic and orthorhombic crystal structure. Notably, the peaks were observed at specific 2θ positions: 35.655° (1 1 1), 41.404° (200), 59.991° (220), 71.78° (311), and 75.52° (222). The curve exhibited consistency with the 3C-SiC polytype, as the peak positions match well with the JCPDS card (reference number 29–1129) for this

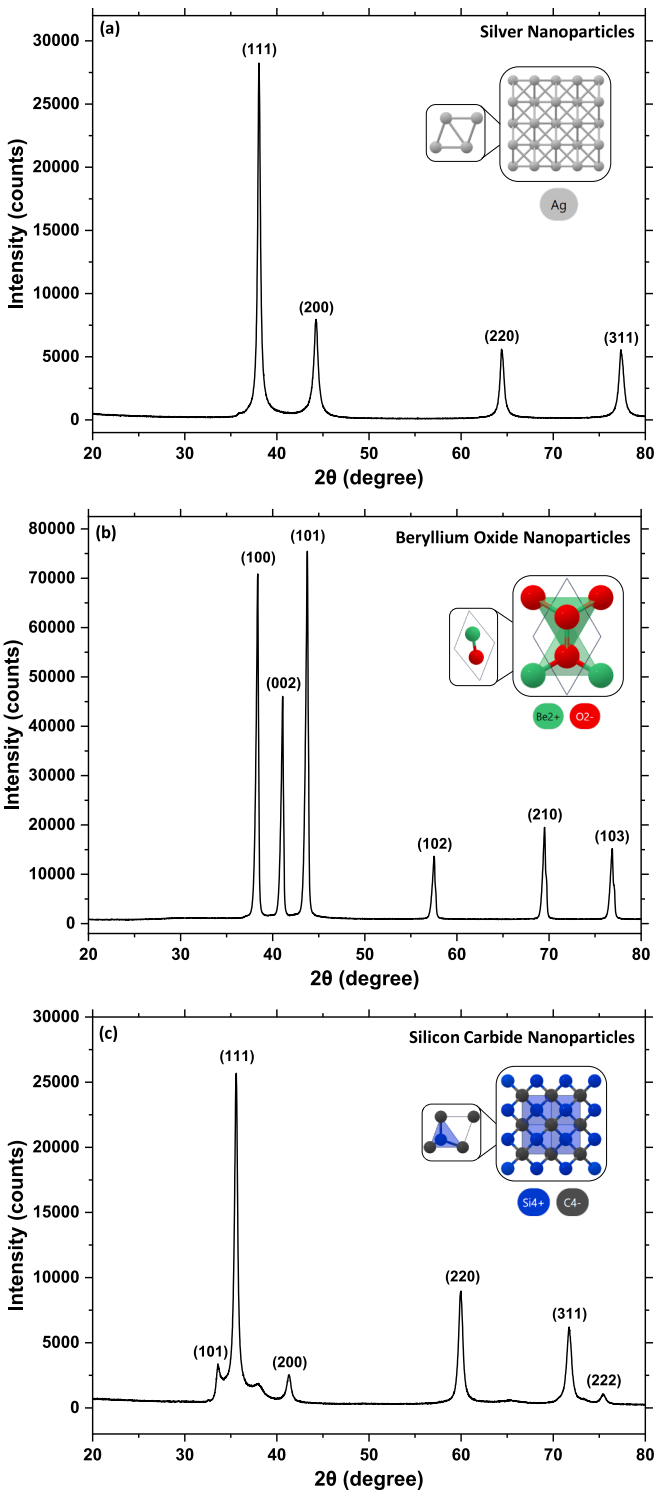

Fig. 8. X-ray diffraction patterns of (a) silver nanoparticles, (b) beryllium oxide nanoparticles, and (c) beta-phase silicon carbide nanoparticles.

material. In this case, the lattice parameter is calculated to be about 4.36 Å, which is in good agreement with the reported value for 3C-SiC. The analysis revealed a unit cell volume of 82.7 Å^3, and the density of the substance was determined to be 3.15 g/cm^3. Sultan et al. [36] investigated the X-ray diffraction (XRD) pattern of silicon carbide across a temperature range of 25 °C to 800 °C. The observed curve trend aligned with the findings of the present study.

To determine the average crystallite size from the peak widths

observed in the XRD pattern a well know Scherrer equation was employed [37,38]. Crystallite size refers specifically to the size of the individual crystalline domains within the nanoparticle. Nanoparticles are often composed of crystalline materials, and the crystallites are the repeating, ordered structures within the particles. The Scherrer equation Eq. (1), widely employed in numerous studies, establishes a mathematical correlation among peak width, X-ray wavelength, and crystallite size. It is commonly utilised to estimate the crystallite dimensions from XRD data.

$$particlesize(d_p) = \frac{\xi\lambda}{\beta\cos\theta} \quad (1)$$

where d_p is the crystallite size, ξ is a constant, λ is the wavelength of the X-rays (1.5406 Å for Cu-Kα radiation), β is the full width at half maximum of the peak, and θ is the Bragg angle.

Applying the Scherrer equation, the calculated crystalline size of silver nanoparticles was determined to be 16.63 nm. However, for beryllium oxide and silicon carbide, the calculated crystalline size was 23.12 nm and 17.19 nm respectively.

4.2. Transmission Electron Microscopy (TEM)

To further analyse the particle morphology, nanoparticles were subjected to Transmission Electron Microscopy (TEM) JEOL JEM-1400 Plus instrument. This powerful analytical technique allows for high-resolution imaging of nanoparticles, enabling detailed examination of their size, shape, and structural characteristics. Fig. 9 presented the TEM images showcasing three distinct types of nanoparticles under investigation in this study.

In the left column, the TEM images depicted the spherical morphology of Ag nanoparticles, which exhibited a tendency to form agglomerates or clusters comprising multiple individual nanoparticles. These agglomerates varied in size and degree of agglomeration. They exhibit a wide size distribution, with some particles appearing quite large (around 40 nm) and others being much smaller (below 20 nm). The particles seem to be agglomerated or aggregated, forming irregular clusters. Moving to the middle column, TEM images illustrated BeO nanoparticles. The beryllium oxide nanoparticles have a more distinct and well-defined shape compared to the silver nanoparticles. They appear as irregular hexagonal with particle sizes ranging from approximately 85 to 140 nm. Although BeO nanoparticles also exhibited a tendency to form agglomerates, their propensity for agglomeration was comparatively lesser than that observed in Ag nanoparticles. Lastly, in the right column, the SiC nanoparticles exhibited a wider range of shapes and sizes compared to the other nanoparticles. Some particles appear as distinct, well-defined shapes, while others have more irregular shapes. Notably, SiC nanoparticles demonstrated a unique tendency to form agglomerates in the form of chains, with connections between particles appearing weaker compared to those observed in Ag and BeO nanoparticles.

It is imperative to consider the sample preparation process, which involves sonication. During this process, some particles experienced breakdown, resulting in the generation of smaller particles. Consequently, the morphology of parent particles underwent alteration, with the emergence of child particles exhibiting smaller sizes. This phenomenon is particularly evident in the TEM images, where irregularities in particle shape and size can be observed.

4.3. Nanofluid stability and particle size distribution

The stability and particle size distribution of the nanofluids were assessed using a Malvern Zetasizer, providing crucial insights into their colloidal behaviour and dispersion characteristics [39,40]. Zeta potential characterizes the intensity of electrostatic repulsion among particles

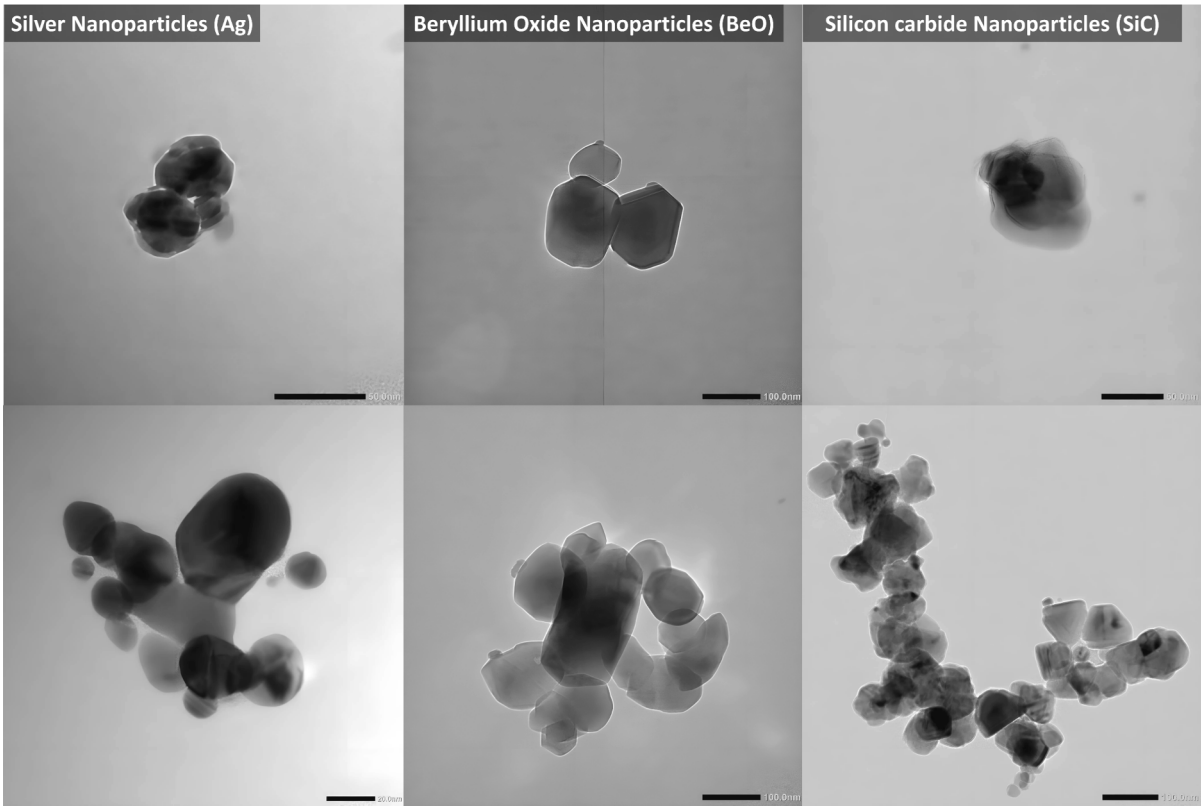

Fig. 9. Transmission electron microscopy (TEM) images of silver, beryllium oxide, and beta-phase silicon carbide nanoparticles (left to right columns).

suspended in a fluid medium. To perform the analysis, the sample was contained within a specialized DTS 1070 cell, designed for assessing zeta potential in controlled environments. This cell is particularly well-suited for evaluating emulsions, suspensions, and other samples where conventional cuvettes may be inadequate. During the measurement process, an electric field was applied to the sample within the DTS 1070 cell. The instrument then assessed the velocity of particles as they responded to this electric field. This velocity is directly linked to the zeta

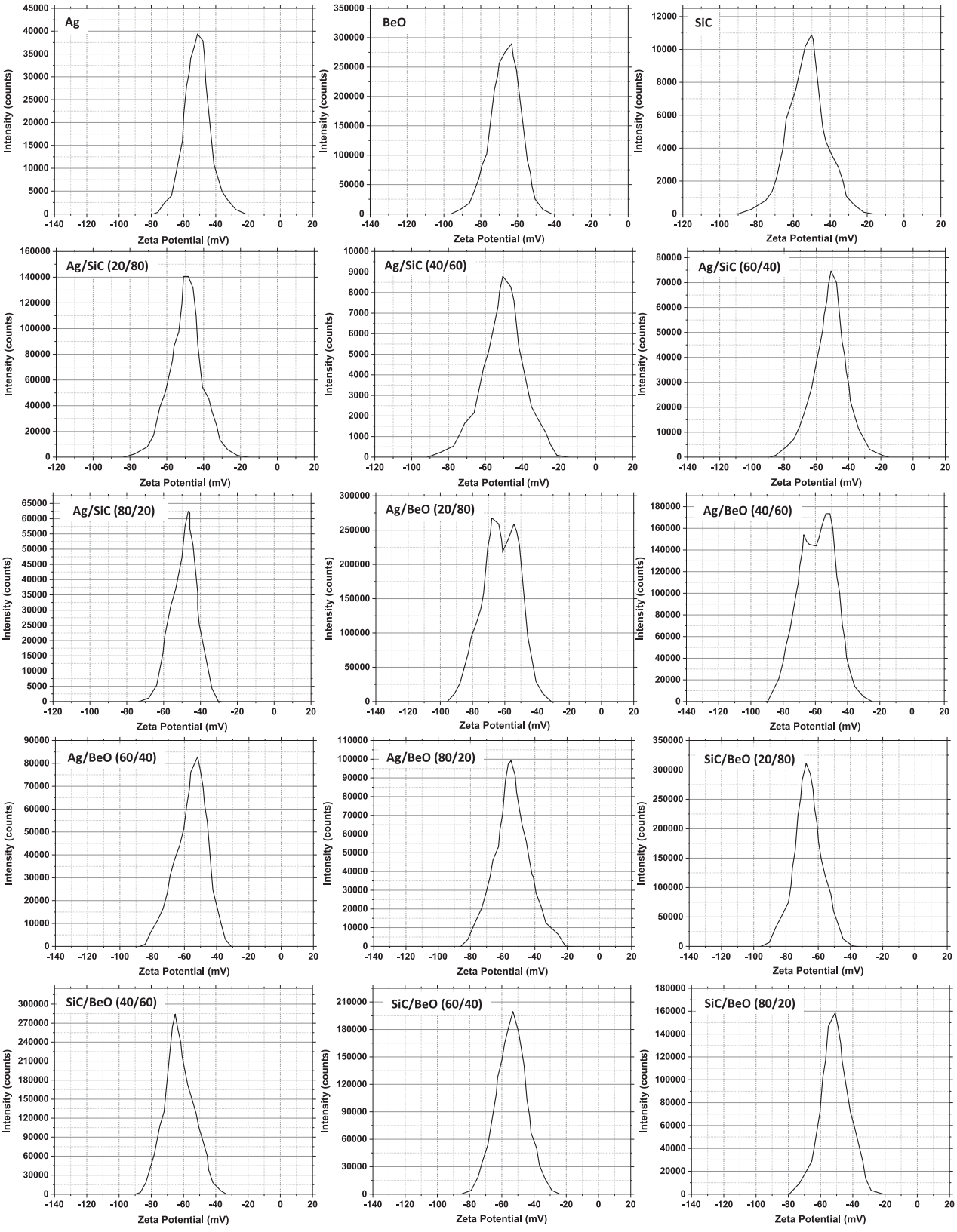

Fig. 10. Zeta potential analysis of simple and hybrid nanofluids at different mixing ratios.

potential, typically calculated using the Smoluchowski equation or similar models. The instrument's software analyses the data collected from the scattered light to determine the zeta potential of the particles in the nanofluid.

Zeta potential analysis was conducted on both simple and hybrid nanofluid samples just after the sonication, revealing values within the range of −45 to −75 mV, as shown in Fig. 10. This range indicates a high level of stability in the nanofluid. In the context of particle suspension, a zeta potential exceeding ± 30 mV is generally considered indicative of good stability, as supported by existing literature [41]. The negative values observed indicate that the nanoparticles possess a net negative surface charge. Factors such as nanoparticle surface chemistry, the types of ions in the solution, surface-active agents, and the pH of the medium, can contribute to the acquisition of a negative charge by the particles. Several studies have also reported negative zeta potential values for these nanofluids [42–44].

Comparing the nanofluids containing different nanoparticles, it was observed that the zeta potential value of BeO nanofluid is better compared to Ag and SiC nanofluids. However, a more extended observation revealed an interesting trend. However, BeO nanoparticles showed a tendency to settle down earlier, primarily attributable to their larger size, posing a significant limitation on the stability over time. The observed limitations in the stability of individual nanofluids, such as BeO nanofluids, underscore the increasing interest in hybrid nanofluids. By combining particles with diverse properties and morphologies, hybrid nanofluids offer the potential to enhance the overall performance of the fluid. In contrast, if larger-sized denser silver nanoparticles were utilized instead of BeO nanoparticles, it would likely have a detrimental effect on the stability of the nanofluid and unsuitable for hybrid formulations.

The hybrid nanofluids displayed varying patterns based on the composition ratios. The Ag/SiC hybrid nanofluids showed distinct peaks corresponding to the individual nanoparticle components, with the peak heights and positions influenced by the ratio of Ag to SiC. It was noted that the Ag/SiC hybrids exhibited a dominant peak around −50 mV. The Ag/BeO hybrid nanofluids exhibited broader peaks compared to the Ag/SiC counterparts, likely due to the broader distribution of BeO nanoparticles. As the ratio of BeO increased, the peak shifted towards more negative zeta potential values, indicating the influence of BeO's higher zeta potential. Finally, the SiC/BeO hybrid nanofluids displayed patterns similar to the Ag/BeO samples, with the peaks becoming broader and shifting towards more negative zeta potential values as the BeO ratio increased.

To investigate the phenomenon of particle clustering or agglomeration and its impact on particle size following suspension, additional particle size analysis was conducted utilising the Malvern Zetasizer instrument. Fig. 11 shows the size distribution of suspended particles in various nanofluid samples after 7 days of fluid preparation. The results revealed the formation of particle clusters or agglomerates, leading to an increase in the effective particle size compared to the initial nanoparticle dimensions.

For the monometallic nanofluid, the Ag sample exhibited a slightly asymmetric peak with a Z-average particle size of 218.4 nm, indicating the presence of relatively uniform and moderately sized agglomerates, significantly larger than the initial 10–40 nm Ag nanoparticles. The presence of a smaller side peak at the right indicates the existence of a small fraction of larger agglomerates or aggregates in the Ag nanofluid suspension. The SiC nanofluid displayed a similar narrow peak with a Z-average size of 230.9 nm, suggesting the formation of agglomerates approximately 4–5 times larger than the initial 45–55 nm SiC nanoparticles. While the BeO nanofluid showed a broader peak with a Z-average size of 404.3 nm, with the agglomerates being only 2–4 times larger than the initial 85–140 nm BeO nanoparticles.

In the case of hybrid nanofluids containing a blend of Ag and SiC nanoparticles (Ag/SiC), narrow peaks were observed across various mixing ratios, instead of a 20:80 ratio. The Ag/SiC (20:80) hybrid nanofluid exhibits a slightly flattened peak with a Z-average particle size of 223.8 nm. Additionally, the appearance of a small side peak indicates the presence of Ag nanoparticles within the hybrid nanofluid. As the proportion of Ag nanoparticles increases in the Ag/SiC (40:60) hybrid nanofluid, the peak becomes slightly narrower, with a Z-average size of 194.3 nm. This reduction in the average agglomerate size could be attributed to the existence of more Ag nanoparticles, however, a small proportion of larger-sized aggregates was also detected. The Ag/SiC (60:40) hybrid nanofluid displays a similar narrow peak to the previous composition, with a Z-average size of 191.8 nm. The peak shape and size distribution suggest a more homogeneous agglomeration pattern with a higher Ag content. Finally, for Ag/SiC (80:20) hybrid nanofluid, where Ag is the predominant component, the peak becomes slightly broader, with a Z-average size of 221.0 nm. This broadening of the peak could be attributed to the increased interactions between the higher concentration of Ag nanoparticles, leading to a slightly wider distribution of agglomerate sizes.

In the Ag/BeO (20:80) hybrid nanofluid, a slightly sharper peak was discerned in comparison to Ag/SiC (20/80) hybrid nanofluid, with a Z-average particle size of 223.3 nm. With a rise in the concentration of Ag nanoparticles within the Ag/BeO (40:60) hybrid nanofluid, the distribution curve covered a broader range due to the augmentation of the smaller size of Ag nanoparticles, with a Z-average size of 224.2 nm. However, small peaks were also observed with the increasing proportion of Ag due to the tendency of the Ag nanoparticles to agglomerate. Analogous to the Ag/SiC (80:20) composition, a small peak was also detected at the smaller size end when the proportion of Ag reached 80 %.

The SiC/BeO hybrid nanofluids exhibited unimodal size distribution curves across all composition ratios instead of a small peak observed for 20:80 sample at the larger size end, as depicted in Fig. 11. In the SiC/BeO (20:80) composition, the average particle size was found to be 271.8 nm, with a relatively narrow distribution curve. As the proportion of SiC increased in the SiC/BeO (40:60) hybrid nanofluid, the average particle size decreased to 246.0 nm. Interestingly, the distribution curve appeared slightly broader compared to the 20:80 composition, suggesting a marginally wider range of particle sizes present in the sample. Subsequently, in the SiC/BeO (60:40) hybrid nanofluid, the average particle size decreased to 232.7 nm, further decreasing with the increasing SiC content. Additionally, the distribution curve slightly shifted towards smaller particle sizes. Finally, with a slight decrease in particle size, while maintaining the curve shape for the SiC/BeO (80:20) hybrid nanofluid, the average particle size was recorded to be 230.0 nm.

It is concluded that the hybrid nanofluids exhibit smaller agglomerate sizes compared to unitary nanofluids due to the unique interplay of different particle characteristics within the solution. The inclusion of nanoparticles, each differing in size, shape, and material properties, introduces heterogeneity that disrupts the natural tendency of particles to cluster together into larger agglomerates. In unitary nanofluids, where all the particles are of the same type, the forces of attraction, such as van der Waals forces, are stronger and more uniform. This leads to a greater likelihood of large agglomerate formation as similar particles tend to stick together more readily. In contrast, hybrid nanofluids

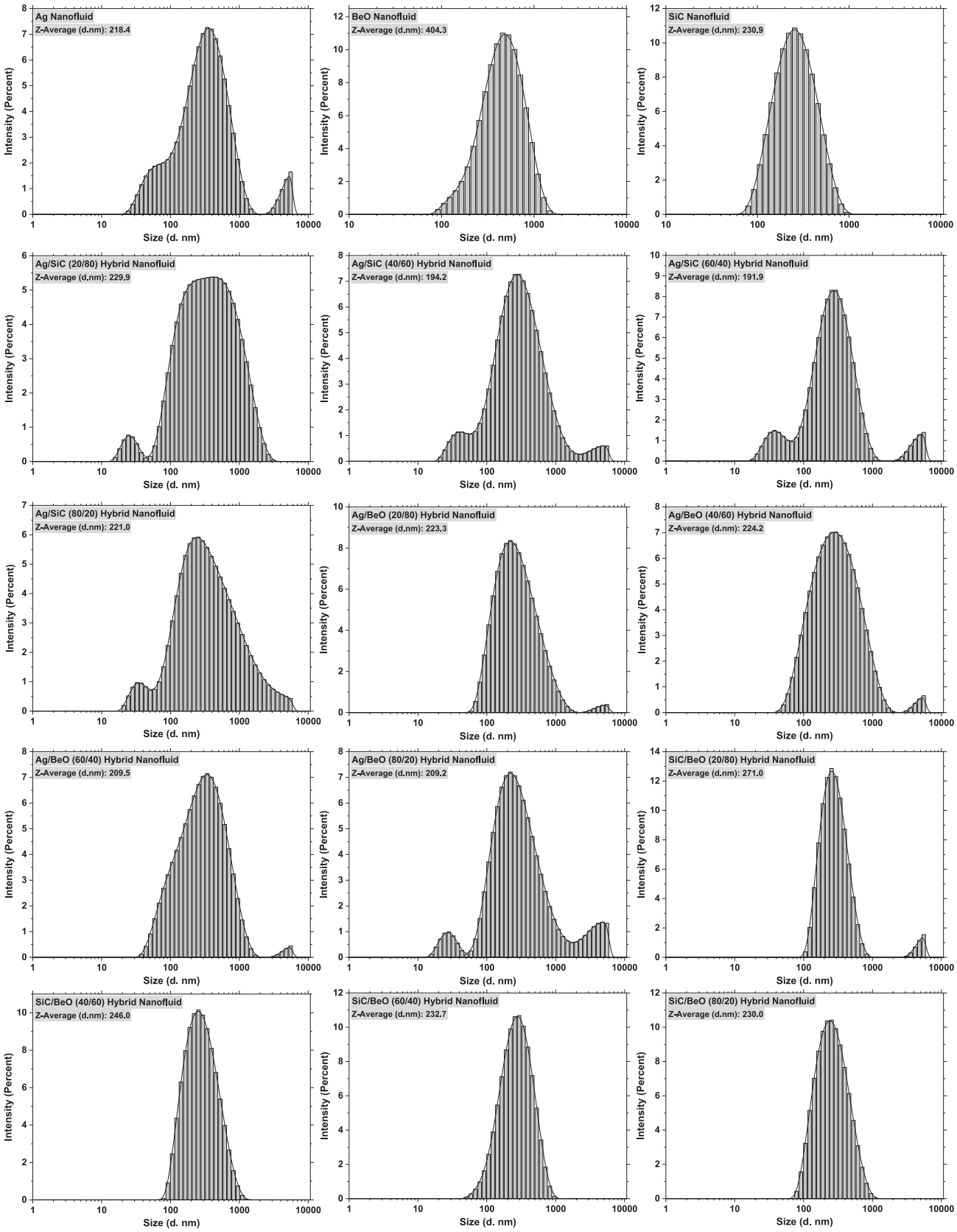

Fig. 11. Particle size distribution curves showing the Z-average particle sizes of simple and hybrid nanofluids at different mixing ratios after 7 days of fluid preparation.

benefit from the diversity of particle sizes and shapes, which creates an uneven distribution of attractive forces. This irregularity weakens the overall attraction between particles, making it easier to prevent large clusters from forming.

Another important factor in the formation of smaller agglomerates in hybrid nanofluids is the synergistic effect of the different materials involved. For example, when smaller particles such as Ag nanoparticles are combined with larger ones like SiC or BeO, the overall balance of forces within the fluid is altered. The smaller particles can help fill the gaps between the larger ones, leading to a more uniform and dispersed suspension. This reduces the tendency of the larger particles to form dense clusters and allows for a more stable distribution of particle sizes. As a result, hybrid nanofluids tend to have a smaller Z-average particle size for agglomerates compared to those formed in unitary nanofluids. Over time, hybrid nanofluids also show improved stability compared to unitary systems. Larger particles like BeO, which may otherwise settle out of suspension in a unitary fluid, are more stable when combined with smaller particles in a hybrid formulation. The different particle types complement each other, reducing the probability of sedimentation and promoting long-term stability. This enhanced stability directly impacts the particle size distribution, as agglomerates that do form are smaller and more uniformly dispersed within the fluid. Therefore, the combination of varied particle types in hybrid nanofluids not only improves thermal and fluidic properties but also results in smaller, more stable agglomerates compared to unitary nanofluids.

These findings highlight the complexity of agglomeration behaviour in nanofluids, where the initial nanoparticle size, composition, and relative proportions in hybrid systems can significantly impact the effective particle size distribution in the suspension. Further investigation into the underlying mechanisms driving the observed agglomeration patterns and their implications for the stability and performance of these nanofluids is warranted.

5. Results and Discussion

5.1. Thermal conductivity

The thermal conductivity of nanofluids, which are suspensions of nanoparticles in a base fluid, is a crucial property that significantly impacts their heat transfer capabilities. The transient plane source (TPS) technique, also known as the hot disk (HD) or Gustafsson probe, is a well-know and accurate method for measuring the thermal conductivity of fluids [45,46]. In this study, the thermal conductivities of water and nanofluid samples were determined using the Hot Disk 2500S thermal constant analyser. The analyser employs a sensor element designed in the configuration of a double spiral, served a dual purpose as a heat source for elevating the sample's temperature and as a resistance thermometer for capturing the temporal evolution of the temperature increase in the heat source itself. The sensor element is constructed with a fine nickel foil, around 10 μm in thickness, configured into a double spiral pattern. Both sides of the spiral are encased in an insulating layer of Kapton, a polyimide material. The meticulous design of this probe is centred around the optimisation of the heating area and length scale for a given sample size. This optimisation ensures a close alignment between the physical model employed and the actual experimental geometry. Notably, the probe's intricate design facilitates the maximization of heating efficiency, thereby enhancing the accuracy and reliability of the thermal conductivity measurements undertaken in our research. The setup comprises a constant temperature bath, a thermal constants analyser, and a purpose-built liquid sample holder. The unique design of the sample holder serves the crucial function of encapsulating the liquid within a confined cell or chamber. The sensor probe is vertically immersed in the liquid sample, and strategically positioned to avoid contact with the cell walls, thereby mitigating the potential impact of convection during measurements. The particularly engineered design of sample holder not only facilitates stable temperature conditions but also effectively eliminates the potential impact of evaporation, given the absence of direct exposure of the liquid to ambient air. To acquire data across various temperature points, the sample holder is positioned within the thermal water bath, facilitating systematic temperature control and enabling the comprehensive investigation of thermal properties under diverse conditions. To facilitate the measurements, a sensor with a radius of 2.001 mm (designated as sensor Kapton 7577) was selected. The experimental setup involved applying a heating power of 60 mW and a measurement time of 2 s.

The uncertainty of the thermal conductivity measurements in this study was evaluated based on both the instrument specifications and the precision of the experimental procedures. The manufacturer specifies a measurement uncertainty of ± 5 % for the TPS method, which reflects the overall expected range of potential deviations in the reported thermal conductivity values. Despite this inherent uncertainty, a rigorous approach was adopted to minimize experimental errors and enhance the precision of the measurements.

To enhance precision, three measurements were taken at each temperature point and reported the average value to mitigate the influence of random errors. The standard deviation of the measurements for fluid samples was found to be less than 0.7 %, which indicates a high level of precision in the data collected. This standard deviation is within the acceptable range and suggests that the variability between repeated measurements was minimal. Additionally, the system was calibrated using a stainless steel sample provided by the manufacturer. The standard deviation for these calibration measurements was less than 0.5 %, demonstrating that the setup was well-tuned and capable of providing reliable data. The study conducted by Sundberg et al. [47] reported that the standard deviation for thermal conductivity measurements using the TPS method was remarkably low, with most samples showing deviations of less than 0.1 %.

To validate the experimental setup, the thermal conductivity of distilled water was measured across a temperature range of 15 °C to 45 °C. The obtained results were subsequently compared with reference values for distilled water, as measured and supplied by Hot Disk [48]. The results showed a good agreement between the experimental values and the provided values, although minor deviations were observed, likely attributable to inherent discrepancies in water properties, as depicted in Fig. 12.

Several studies have reported the influence of surfactants on the thermal conductivity of nanofluids [49,50]. To investigate this, a study was carried out to examine the thermal conductivity of freshly prepared samples with those measured after 72 h. The measurements were

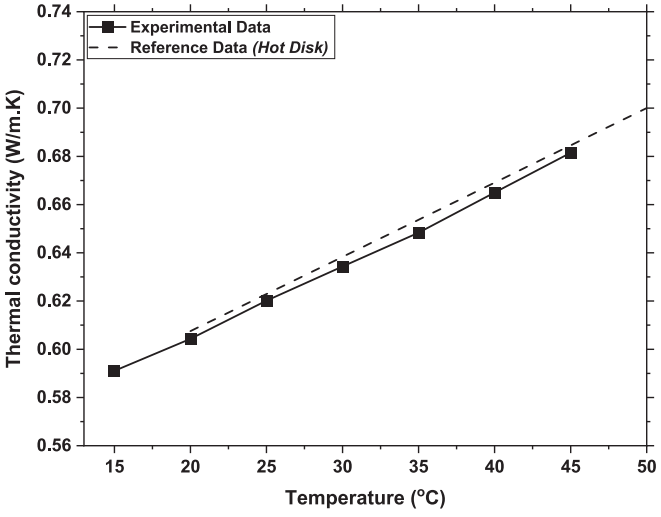

Fig. 12. Thermal conductivity of distilled water as a function of temperature, comparison of experimental data with reference data.

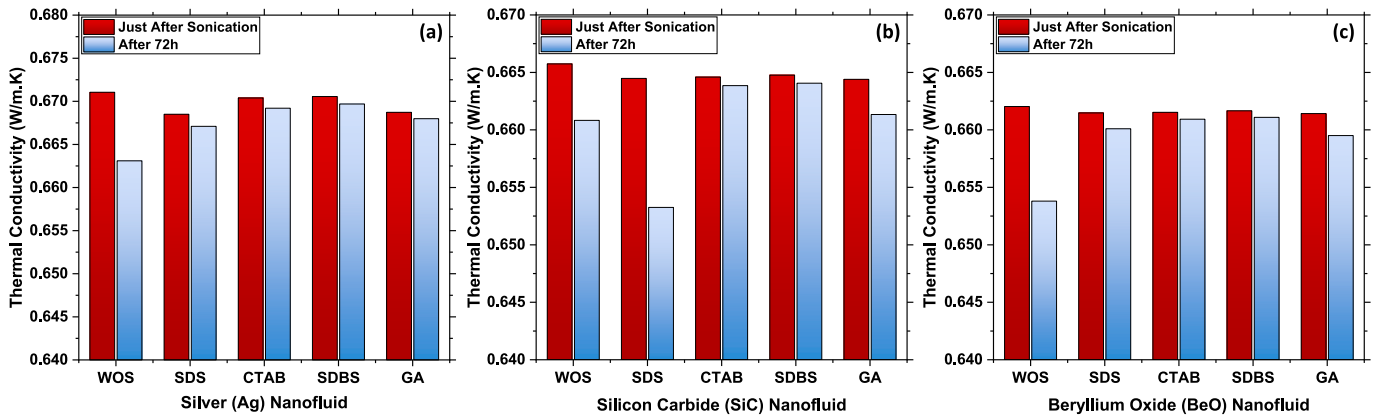

Fig. 13. Thermal conductivity of nanofluids just after sonication and after 72 h. (a) Silver nanofluid, (b) Silicon Carbide nanofluid, (c) Beryllium Oxide nanofluid.

performed at 35 °C, and the results are presented in Fig. 13. According to the results obtained immediately after sonication, a noticeable variation was observed in the thermal conductivity values between the surfactant-free and surfactant-added fluid samples. Notably, SDBS surfactant demonstrated better stability, with less pronounced changes in thermal conductivity compared to others. Subsequent measurements after 72 h displayed diverse trends among different nanofluid samples. The surfactant-free silver nanofluid exhibited a considerable decrease in thermal conductivity, whereas this reduction was less pronounced for samples containing SDBS and CTAB surfactants. Specifically, SDBS showed promising stability, while SDS proved less suitable for silver nanoparticle-containing fluids. Although GA performed better than SDS, it still fell short compared to SDBS for silver nanofluids.

As anticipated for silicon carbide nanofluids, a slight decrease in thermal conductivity was observed upon the addition of various surfactants. The thermal conductivity values were found to be in the following sequence with slight changes WOS > SDBS > CATB > SDS > GA. Notably, SDS surfactant exhibited a distinct behaviour with silicon carbide nanoparticles. After 72 h, the sample containing SDS surfactant experienced a significant reduction in value, indicating an adverse effect on stability. The surfactant-free sample exhibited better stability and higher thermal conductivity compared to the SDS sample. Within a week, all particles had settled, leaving the water clear. The thermal conductivity of the SDS sample decreased from 0.664 W/m•K to 0.653 W/m•K within 72 h. However, nanofluid samples containing SDBS and CTAB surfactants exhibited comparatively better values after 72 h, measured to be 0.664 W/m•K and 0.664 W/m•K, respectively. As for GA, although the upper layer of the sample began clearing after 72 h, a reduction in thermal conductivity was observed from 0.664 W/m•K to 0.661 W/m•K.

The beryllium oxide solution exhibited lower stability compared to others, but the addition of surfactants played a crucial role in stabilizing the suspension. According to the results collected just after the sonication, the thermal conductivity value of surfactant free sample was slightly higher than others like silver and silicon carbide suspensions. However, after 72 h, the upper layer of the fluid became transparent as particles settled, resulting in a marginal decrease in thermal conductivity from 0.662 W/m•K to 0.6538 W/m•K. The addition of SDBS surfactant was found to enhance stability and mitigate the reduction in thermal conductivity by reducing particle agglomeration and settling. The CTAB surfactant followed closely, offering improved stability albeit with slightly lower thermal conductivity than SDBS. A decrease in thermal conductivity values was noted for SDBS and CTAB samples, from 0.6626 to 0.6611 W/m•K and 0.6615 to 0.6609 W/m•K, respectively. Gum Arabic was found to be unsuitable for beryllium oxide nanofluids. The findings of this study strongly advocate for the use of surfactants in the preparation of beryllium oxide solutions to ensure effective stability maintenance.

This study reveals that the effectiveness of surfactants varies depending on the nanoparticles involved. SDBS and CTAB exhibit superior performance in some cases, but for other particles, GA or SDS may offer better stability. This suggests that the choice of surfactant should be tailored to the specific nanoparticles being used. Furthermore, ongoing investigations are exploring additional surfactants and combinations thereof to determine their effects on stability and thermal performance. Future research endeavours may focus on evaluating additional surfactants and assessing the synergistic effects of surfactant combinations to further optimize nanofluid properties.

Particle concentration is the other significant factor influencing the thermal conductivity of nanofluids [51,52]. Understanding how changes in particle concentration affect thermal conductivity is essential for optimizing nanofluid formulations for various applications. A study was undertaken to investigate the influence of particle concentration on thermal conductivity within the range of 0.01 vol% to 0.025 vol%. This range was selected considering the importance of stability, particularly in applications such as thermal management of electronic components, especially for mini and microchannel heat sinks. Higher concentrations of particles can lead to various challenges. These include increased pressure drop and pumping power, as well as the risk of particle agglomeration leading to blockages within the channels, especially in cases where the flow is predominantly laminar. Such blockages can result in localized heating, potentially causing damage to the entire system.

Fig. 14 illustrates the impact of particle concentration on the thermal conductivity of various nanofluids. As the concentration of nanoparticles increased, there was a consistent rise in thermal conductivity enhancement. This enhancement can be attributed to factors such as increased particle-packing density, enhanced Brownian motion, and greater surface area for heat transfer. The major contributing factor to the increase in thermal conductivity with higher concentrations is the inherently higher thermal conductivity of nanoparticles, amplified by the larger number of particles present in the nanofluid at higher

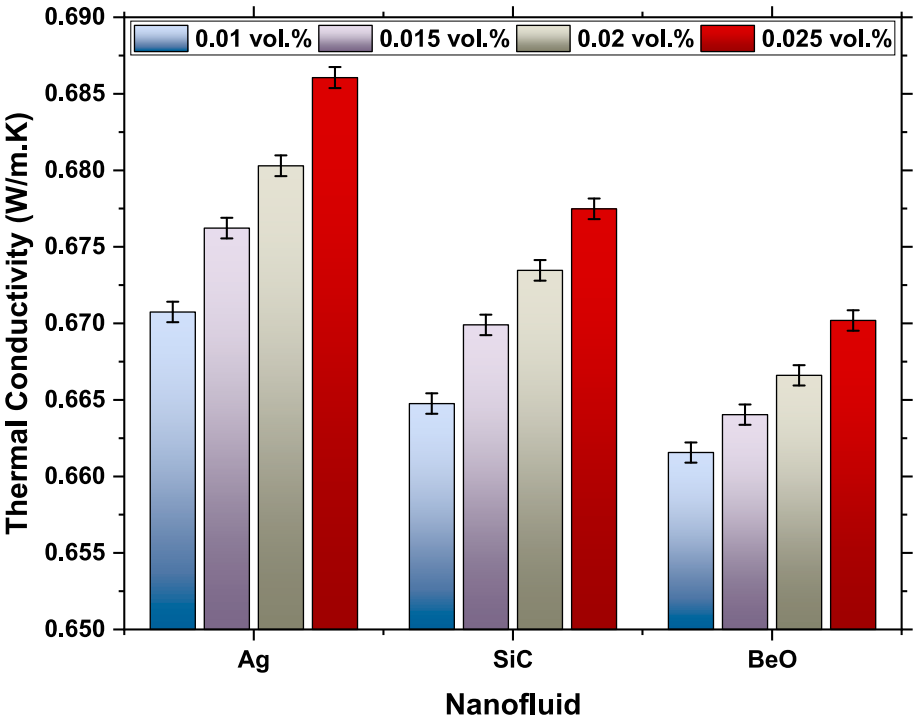

Fig. 14. Variation of thermal conductivity with particle concentration for different nanofluids.

concentrations. As more nanoparticles are dispersed within the fluid, they contribute more significantly to enhancing heat transfer capabilities. Additionally, the greater interaction between nanoparticles and the surrounding fluid facilitates more efficient heat transfer pathways, leading to higher overall thermal conductivity.

The fluid containing silver nanoparticles outperformed at all concentrations because of their better thermal properties. At 0.025 vol%, silver nanofluid achieved the highest thermal conductivity of 0.6861 W/m•K, showcasing its excellent heat transfer capabilities. For silicon carbide nanofluid, the thermal conductivity exhibited an increase with the augmentation of particle concentration, however, the enhancement was slightly lower compared to silver nanofluid. At a 0.01 vol% concentration of silicon carbide nanoparticles, the thermal conductivity of the nanofluid was measured to be 0.6707 W/m•K. This represented an enhancement of approximately 2.53 % over pure water. When the nanoparticle concentration was increased to 0.025 vol%, the thermal conductivity further improved to 0.6861 W/m•K, indicating a 4.49 % enhancement over water. The higher thermal conductivity of silicon carbide nanoparticles, coupled with improved dispersion within the fluid, facilitates enhanced heat transfer, resulting in increased overall thermal conductivity.

In contrast to silver and silicon carbide nanofluids, the thermal conductivity of beryllium oxide nanofluid exhibits a relatively modest increase with increasing particle concentration. At 0.01 vol%, the thermal conductivity is measured to be 0.6616 W/m•K, reaching 0.6702 W/m•K at 0.025 vol%. Despite this increase, the improvement in thermal conductivity is not as significant compared to other nanofluids, with enhancements ranging from 2.035 % to 3.366 % across the concentration range. This may be attributed to the intrinsic properties of beryllium oxide nanoparticles and their interaction with the base fluid. However, even though the enhancement is modest, the presence of beryllium oxide nanoparticles still helps improve the fluid's ability to transfer heat.

Fig. 15 presented the variation of thermal conductivity with temperature for both simple and hybrid nanofluids, measured at 0.025 vol% concentration over a temperature range of 15 – 45 °C. Notably, all samples exhibited a substantial increase in thermal conductivity as the temperature varied. However, it was observed that at lower temperatures, this increase was less pronounced compared to higher temperatures, with a noticeable acceleration in augmentation beyond 30 °C. This phenomenon may be attributed to the enhanced Brownian motion of nanoparticles at elevated temperatures, leading to improved dispersion and subsequently increased thermal conductivity. Such behaviour holds significant implications, particularly in applications where nanofluids serve as heat transfer fluids, as their performance is inherently linked to their ability to efficiently carry and disperse heat. Moreover, it is noteworthy that hybrid nanofluids, with an optimal mixing ratio, demonstrated superior thermal performance compared to simple nanofluids. This underscores the potential benefits of synergistic nanoparticle combinations, presenting promising avenues for enhancing thermal conductivity and overall performance in various practical applications.

The enhancement values, calculated by comparing the thermal conductivity of silver nanofluid to that of water, reveal a significant improvement in thermal conductivity with the addition of silver nanoparticles. The highest enhancement of 6.95 % was observed at 45 °C, as shown in Fig. 15(a). The SiC nanofluid sample also exhibited a consistent increase in thermal conductivity with rising temperatures. At each temperature point, the thermal conductivity of SiC nanofluid was higher than that of water, indicating the enhancement effect of silicon carbide nanoparticles on heat transfer properties. Comparing silicon carbide

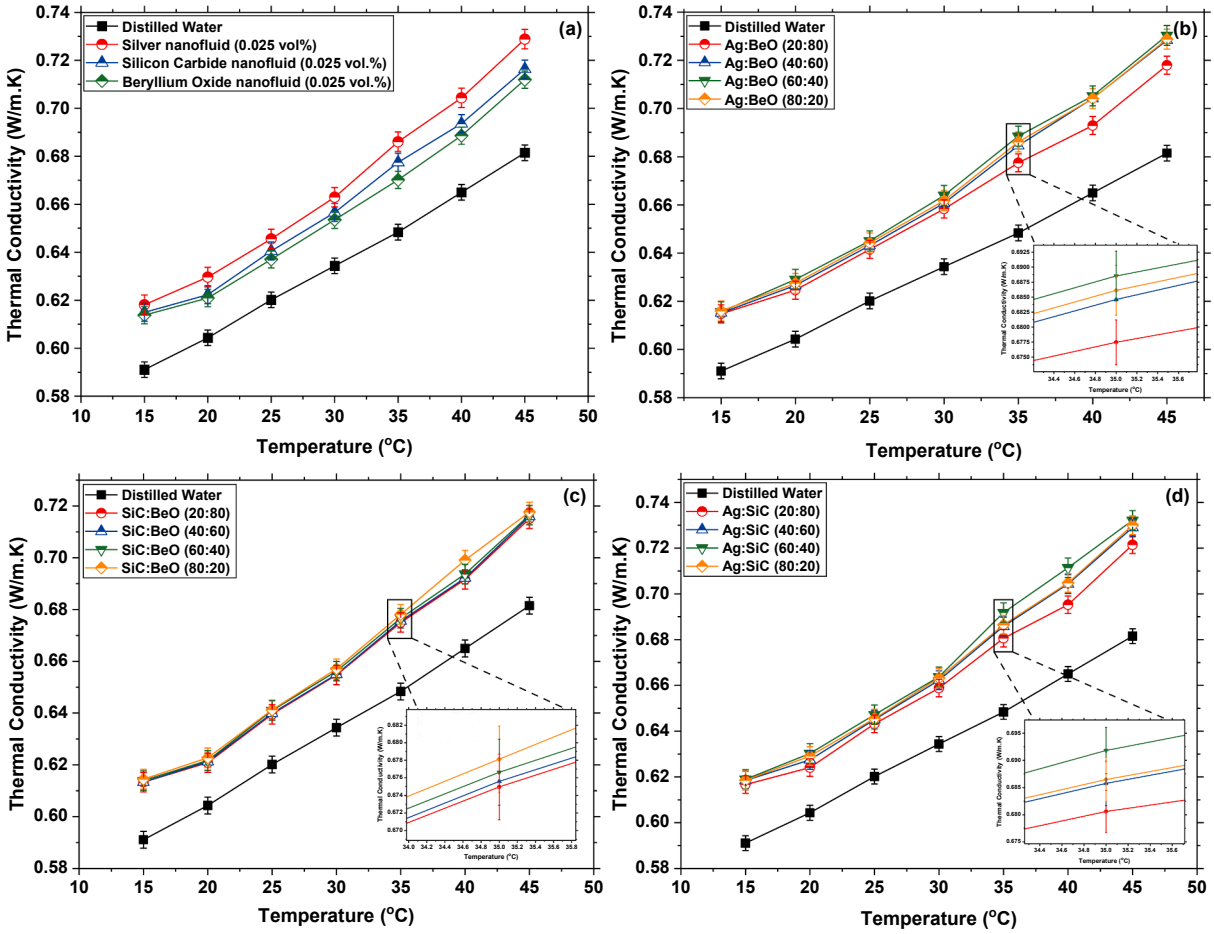

Fig. 15. Thermal conductivity of simple and hybrid at different mixing ratios over the temperature range of 15–45 °C.

nanofluid to silver nanofluid, it was evident that silver nanoparticles generally resulted in higher thermal conductivity values across all temperature points. However, the enhancement values for SiC nanofluid are notably substantial, the maximum improvement was noted to be 5.11 % at 45 °C, indicating that silicon carbide nanoparticles effectively enhance the thermal conductivity of the nanofluid. The sample prepared by suspending BeO nanoparticles consistently exhibited lower thermal conductivity compared to silver and silicon carbide nanofluid across the temperature range. However, despite the lower values, BeO nanofluid still showed a notable enhancement compared to basefluid (water), reaching 4.47 % at 45 °C. The results indicated that while the thermal conductivity of BeO nanofluid may not have reached the levels observed in silver and silicon carbide nanofluids, the addition of beryllium oxide nanoparticles still led to significant improvements in heat transfer properties.

It is important to consider that in this study, the nanofluid samples were all prepared based on volume per cent (vol.%) instead of weight per cent (wt.%). While factors like the thermal conductivity of particles, base fluid, stability, particle size, shape, surfactant, and solution pH are well-known to influence the thermal properties of nanofluids, particle density also plays a significant role [51]. Since density directly affects the number of particles added per unit volume, using particles with lower densities at the same volume fraction results in a greater number of particles. These additional particles act as heat carriers, potentially enhancing the thermal conductivity of the nanofluid. This effect is particularly important for hybrid nanofluids. In these fluids, particles with different thermal conductivities, densities, and crystalline structures are combined. The interplay between these diverse characteristics can lead to synergistic effects, further improving the thermal properties beyond what could be achieved with single-type nanoparticles.

Fig. 15(b) presented the thermal conductivity of silver and beryllium oxide hybrid solutions prepared with different mixing ratios. Across the studied ratios of 20/80, 40/60, 60/40, and 80/20, we observed a consistent trend of thermal conductivity enhancement compared to pure water with a noticeable fluctuation in the values at different mixing ratios. This enhancement, ranging from approximately 3.36 % to 7.17 % compared to water, underscores the effectiveness of incorporating Ag and BeO nanoparticles into the fluid matrix. The observed enhancement trends suggest that certain mixing ratios may yield more favourable thermal conductivity enhancements. Notably, the mixing ratio of 60/40 demonstrated the highest enhancement values. This optimal balance between Ag and BeO nanoparticles likely facilitates synergistic effects, resulting in enhanced thermal conductivity performance. The hybrid solution with a mixing ratio of 20/80 exhibited a maximum enhancement of 5.35 % compared to water, falling between the enhancement values of pure silver and beryllium oxide nanofluids. Following this, the 40/60 solution showed a maximum enhancement of 6.88 %, closer to the enhancement observed in pure silver nanofluids. However, the most

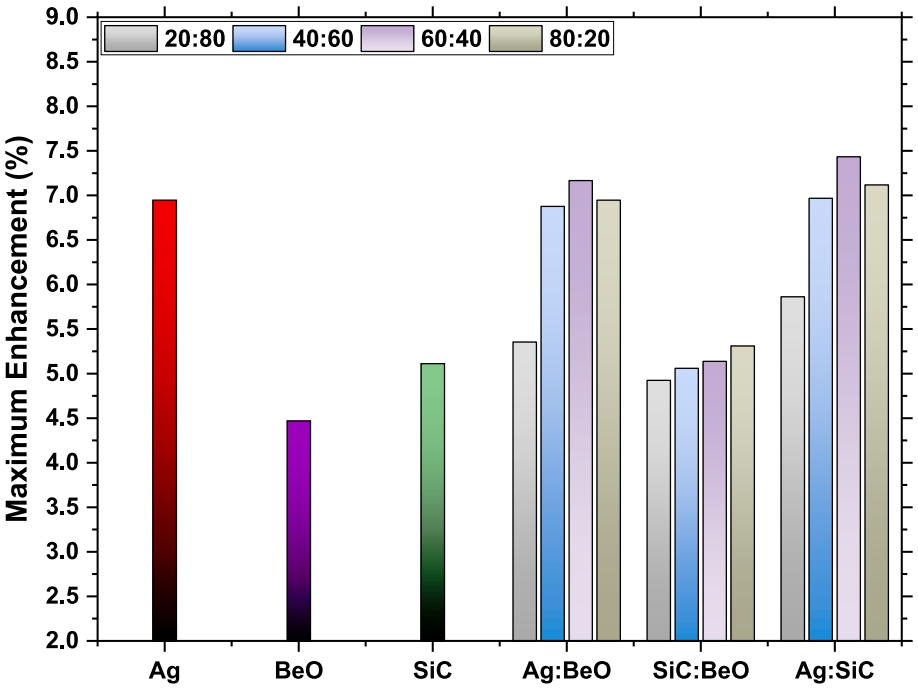

Fig. 16. Maximum thermal conductivity enhancement compared to water for various nanofluids at different mixing ratios.

significant enhancement of 7.17 % was observed at the 60/40 mixing ratio. This increase could be attributed to the combined effects of the nanoparticles' distinct thermal characteristics, density values, crystalline structure, interactions, and suspension behaviours in the fluid. Furthermore, a slight decrease in thermal conductivity enhancement is noted as the mixing ratio shifts from 60/40 to 80/20, aligning the thermal conductivity values more closely with those of pure silver nanofluids. The findings from the investigation of Ag/BeO hybrid suspensions suggest that a mixing ratio of 60/40 represents the optimal concentration for achieving enhanced thermal conductivity.

Similar to the Ag/BeO hybrid suspension, the results obtained from the SiC/BeO suspension suggest that specific mixing ratios can lead to more favourable enhancements in thermal conductivity. Across the range of mixing ratios examined, it was observed that the fluid with a mixing ratio of 80/20 exhibited the highest enhancement in thermal conductivity compared to pure water and individual nanofluids, as depicted in Fig. 15(c). The thermal conductivity was observed to improve with increasing the ratio of SiC and reducing BeO. At the mixing ratio of 20/80, the maximum improvement in thermal conductivity relative to water was 4.92 %, falling between the enhancements observed for pure SiC and BeO nanofluids. For the 40/60 hybrid sample, the thermal conductivity value reached 0.716 W/m•K at 45 °C, with an enhancement of approximately 5.06 %, which was slightly lower and closer to that of the SiC nanofluid. However, the samples with mixing ratios of 60/40 and 80/20 demonstrated higher enhancements compared to others, measuring 5.14 % and 5.31 %, respectively, as shown in Fig. 16. The results indicate that the mixing ratio of 80/20 is optimal for achieving higher thermal conductivity values in SiC/BeO hybrid suspensions.

The results of Ag/SiC hybrid nanofluids, as depicted in Fig. 15(d), further corroborate the observations made in previous cases regarding the differential impact of specific mixing ratios on thermal conductivity enhancement in hybrid suspensions. The hybrid nanofluid with a mixing ratio of 20/80 exhibited a notable enhancement of 5.86 %, elevating its thermal conductivity from 0.617 W/m•K to 0.7216 W/m•K over the temperature range of 15 °C to 45 °C. Although this hybrid suspension demonstrated improved stability and thermal conductivity compared to pure SiC nanofluid, it still fell short of the thermal conductivity achieved by simple silver nanofluid. As the mixing ratio changed to 40/60, a notable enhancement brought the thermal conductivity closer to that of pure silver nanofluid, reaching a maximum enhancement of 6.97 % at 45 °C. Although this solution offers improved stability and cost-effective, its thermal conductivity is comparable to that of simple nanofluids. The hybrid nanofluid suspension with a 60/40 mixing ratio outperformed all, showing an enhancement of 7.43 %. This represents the maximum enhancement observed in this study. As the mixing ratio shifted from 60/40 to 80/20, a slight decrease in enhancement was noted, reaching 7.12 %.

A number of factors elaborated above are responsible for making the hybrid nanofluid preferable over pure nanofluids. It is evident from the results that careful selection of nanoparticle combinations and mixing ratios is crucial in maximising thermal conductivity enhancements in hybrid nanofluids. Based on these findings, it is recommended to utilise the Ag/SiC hybrid nanofluid with a 60/40 mixing ratio for applications requiring enhanced heat transfer efficiency. Further exploration and optimisation of mixing ratios could potentially lead to even greater enhancements in thermal conductivity, offering valuable insights for the design and development of advanced heat transfer fluids.

An analysis was carried out using Design Expert to study the relationship between temperature and thermal conductivity of various nanofluids [53]. In this study, a confidence level of 95 % or a 5 % significance level for the critical P-value was utilized. Through meticulous examination, a quadratic model was established to predict thermal conductivity with high precision, Eq. (2). The quadratic model

Table 2
ANOVA for the quadratic model of thermal conductivity.

Source	Sum of Squares	df	Mean Square	F-value	p-value	Significance of model
Model	0.1531	32	0.0048	1049.5	< 0.0001	Significant
A-Fluid	0.0074	15	0.0005	107.68	< 0.0001	
B-Temperature	0.1439	1	0.1439	31573.93	< 0.0001	
AB	0.0006	15	0	8.87	< 0.0001	
B^2	0.0012	1	0.0012	261.86	< 0.0001	
Residual	0.0004	79	4.56E-06			
Std. Dev.	0.0021		**R^2**	0.9977		
Mean	0.6619		**Adjusted R^2**	0.9967		
C.V. %	0.3225		**Predicted R^2**	0.9949		
PRESS	0.000774		**Adeq Precision**	120.3633		

Table 3
The values of coefficients for the thermal conductivity of fluid samples.

Sample	a	b	Sample	a	b
DW	0.574933	0.000745	SiC/BeO (20:80)	0.585405	0.001183
Ag	0.586206	0.001468	SiC/BeO (40:60)	0.585192	0.001205
SiC	0.586782	0.001193	SiC/BeO (60:40)	0.585659	0.00122
BeO	0.587524	0.001045	SiC/BeO (80:20)	0.584672	0.001305
Ag/BeO (20:80)	0.58795	0.001182	Ag/SiC (20:80)	0.587144	0.001268
Ag/BeO (40:60)	0.581365	0.001569	Ag/SiC (40:60)	0.58487	0.001497
Ag/BeO (60:40)	0.582735	0.001595	Ag/SiC (60:40)	0.583829	0.001642
Ag/BeO (80:20)	0.582755	0.00155	Ag/SiC (80:20)	0.5855	0.001501

considered both the linear and quadratic effects of temperature providing a comprehensive understanding of the phenomenon. This model was subjected to Analysis of Variance (ANOVA) analysis, a powerful statistical tool that dissected the significance of each model term. The ANOVA table provides information on the overall significance of the model and the statistical significance of different terms (A, B, AB, B^2) in the model, as illustrated in Table 2. It revealed that the model as a whole was exceptionally significant, with a p-value < 0.0001, indicating its robustness in explaining variations in thermal conductivity. Furthermore, individual model terms such as A-Fluid, B-Temperature, AB, and B2 exhibited remarkable significance, further validating the model's efficacy.

$$ThermalConductivity(k) = a + bT + 0.000038T^2 \quad (2)$$

here a and b are coefficients representing the intercept and the linear coefficient respectively. The term T^2 represents the quadratic effect of temperature. Each nanofluid sample has its specific values for these coefficients as presented in Table 3.

The standard deviation (Std. Dev.) of the model was calculated to be 0.0021. This value indicates the variability of the data points around the mean. Assessing the model's performance, metrics such as Predicted R^2 and Adjusted R^2 provided insights into the model's goodness of fit, showcasing its ability to accurately capture the relationship between temperature and thermal conductivity. The high values of these metrics, coupled with an Adeq Precision ratio exceeding 120, signified not only a strong signal but also a practical utility of the model in navigating the design space.

The coefficient of determination (R^2) was found to be 0.9977, indicating that approximately 99.77 % of the variability in the thermal conductivity data can be explained by the quadratic model. The Predicted R^2 value of 0.9949 demonstrates strong agreement with the Adjusted R^2 value of 0.9967. With a difference of less than 0.2 between the two metrics, it indicates that the model's predictive power remains consistently high even when applied to new data. The coefficient of variation (C.V. %) of 0.3225 % indicates the relative variability of the thermal conductivity data around the mean. Finally, the PRESS (Predicted Residual Error Sum of Squares) is a measure of the model's predictive performance. It quantifies the difference between predicted values and actual observed values, with lower values indicating better predictive accuracy. In this case, a PRESS value of 0.000774 suggests that the model's predictions closely align with the actual observed data points.

Fig. 17(a) shows the relationship between the experimental thermal conductivity values with the predicted using the ANOVA model. The closer the points lie to the diagonal line, the better the model fits the data. In this case, the data aligns well with the diagonal line, reflecting a satisfactory model fit. The normal probability plot of studentized residuals reveals that the errors associated with the thermal conductivity are approximately normally distributed, Fig. 17(b). This plot is used to assess whether the residuals conform to a normal and independent distribution. The alignment of data points with the straight normal line suggests that the error values associated with the thermal conductivity values are distributed normally. As visualised in the plot, the data points appeared to be reasonably close to the diagonal line, signifying adherence to the expected normal distribution of errors in the model.

The residual plots are utilised to assess the presence or absence of covariance among the errors concerning various independent variables, such as experiment number, prediction values, and time [54]. This analytical approach facilitated the identification of any potential covariance or lack thereof in the response variable. If no discernible pattern is evident in the dispersion plot, it suggests that the errors are covariant. Conversely, if the model's accuracy is affirmed, and acceptance criteria are met, the residuals are expected to demonstrate an unstructured pattern and independence from other variables, including the response variable. This behaviour would indicate the absence of covariance among the errors. As depicted in Fig. 17(c) and Fig. 17(d), no

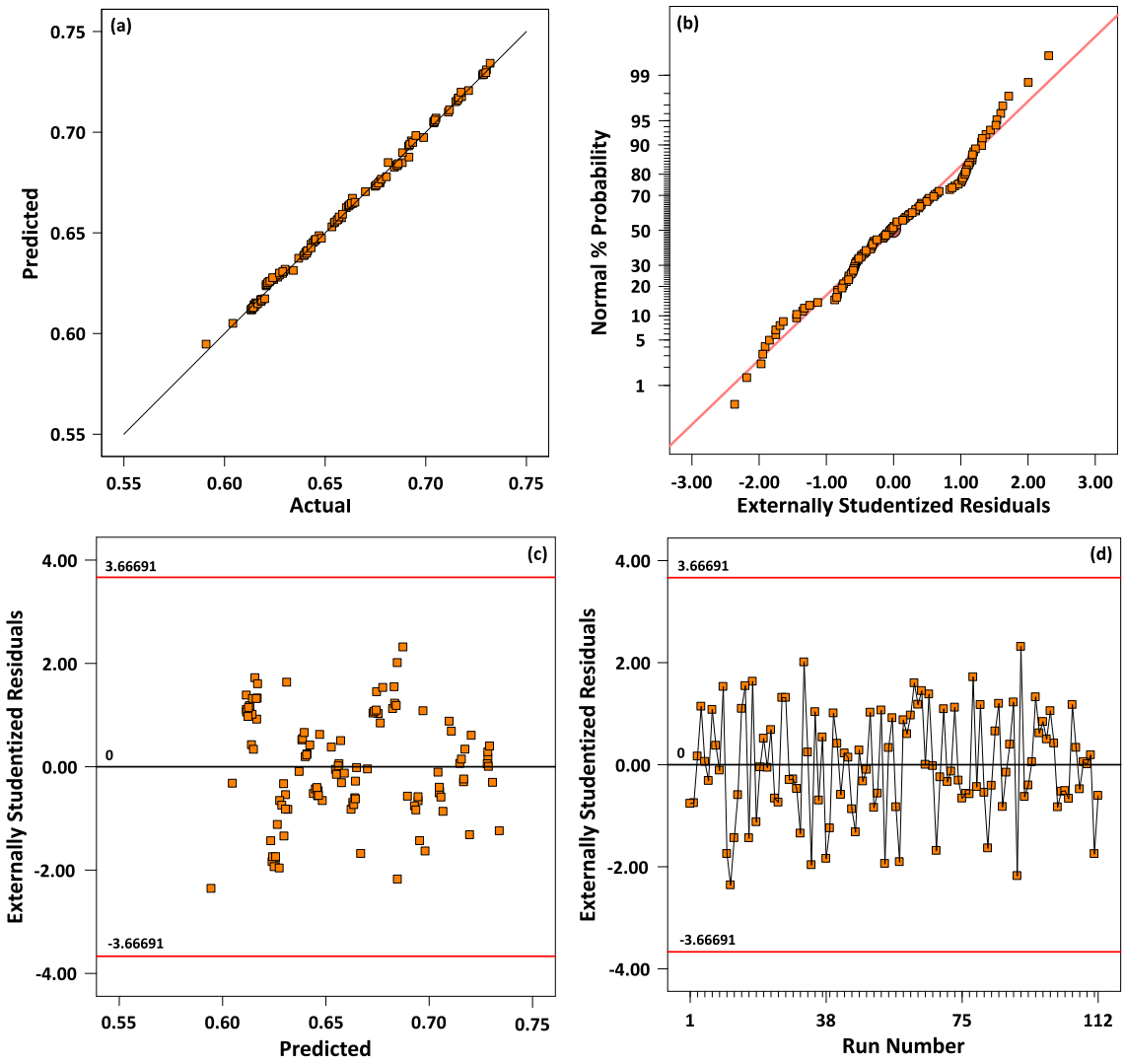

Fig. 17. Thermal conductivity model plots (a) Predicted vs actual values, (b) Normal probability of studentized residuals, (c) Residuals vs predicted values, (d) Residuals vs run number.

conspicuous structures or discernible patterns are evident, with all points falling within the bounds of three standard deviations. Thus, it is inferred that errors exhibit covariance.

In Fig. 18, the thermal conductivity results of silver and Ag/SiC (60:40) nanofluids were compared to the literature values and predictions from classical models. It was found that the classical models such as Maxwell [55] and Hamilton and Crosser [56] failed to predict the values. Mahbubul et al. [57] also observed that experimental values exceeded those predicted by the models of Maxwell, Hamilton-Crosser, and Yu and Choi. These models are now considered outdated and often fail to provide accurate predictions. Consequently, recent studies have focused on experimental methods to better capture the thermophysical properties of nanofluids, which can then be applied to practical systems. The models developed in this study offer accurate predictions of the thermal conductivity of the nanofluid under investigation. Additionally, the results showed that the hybrid combinations used provided better thermal conductivity compared to many oxide-based and oxide-containing nanofluids. Dalkılıç et al. [58] examined the thermal characteristics of water-based CNT-SiO_2 hybrid nanofluids prepared with different mixing ratios. Their findings revealed that at a 0.1 % volume fraction, the maximum enhancement was observed to be approximately 6.16 % for the CNT:SiO_2 (80:20) ratio. Kazemi et al. [59] investigated the thermal conductivity of graphene and silica nanoparticles in both mono and hybrid nano-additive forms. The results revealed that the hybrid nanofluid G-SiO_2 achieved a notable thermal conductivity enhancement of approximately 5 % and 8 % at a concentration of 0.05 % and 0.1 %, respectively, outperforming the individual components. The findings suggested that while pure nanofluid contributed more significantly to thermal conductivity, the hybrid formulation was more cost-effective, making it a viable option for thermal applications. Sreekumar et al. [60] explored the properties of MXene/Carbon-dot hybrid nanofluid, which exhibited superior thermal conductivity and optical characteristics compared to conventional heat transfer fluids. Their findings showed that the thermal conductivity of the Carbon-dot nanofluid at 0.01 wt% and 45 °C was approximately 0.71 W/m·K. Said et al. [61] studied the thermal conductivity of TiO_2/water nanofluids and concluded that fluids prepared with low particle concentrations had a negligible impact on pumping power in heat transfer applications. While TiO_2/water nanofluids demonstrated notable improvements in thermal conductivity and exhibited reasonable stability, challenges such as increased viscosity and particle aggregation over time could affect their long-term performance in heat transfer systems. Zhang et al. [62] found that GPTMS-modified TiO_2/water nanofluids (G-TiO_2) showed better stability and higher thermal conductivity than surfactant-added nanofluids. The thermal conductivity enhancement for G-TiO_2 increased from 4.19 % to 14.28 % as the nanoparticle concentration rose from

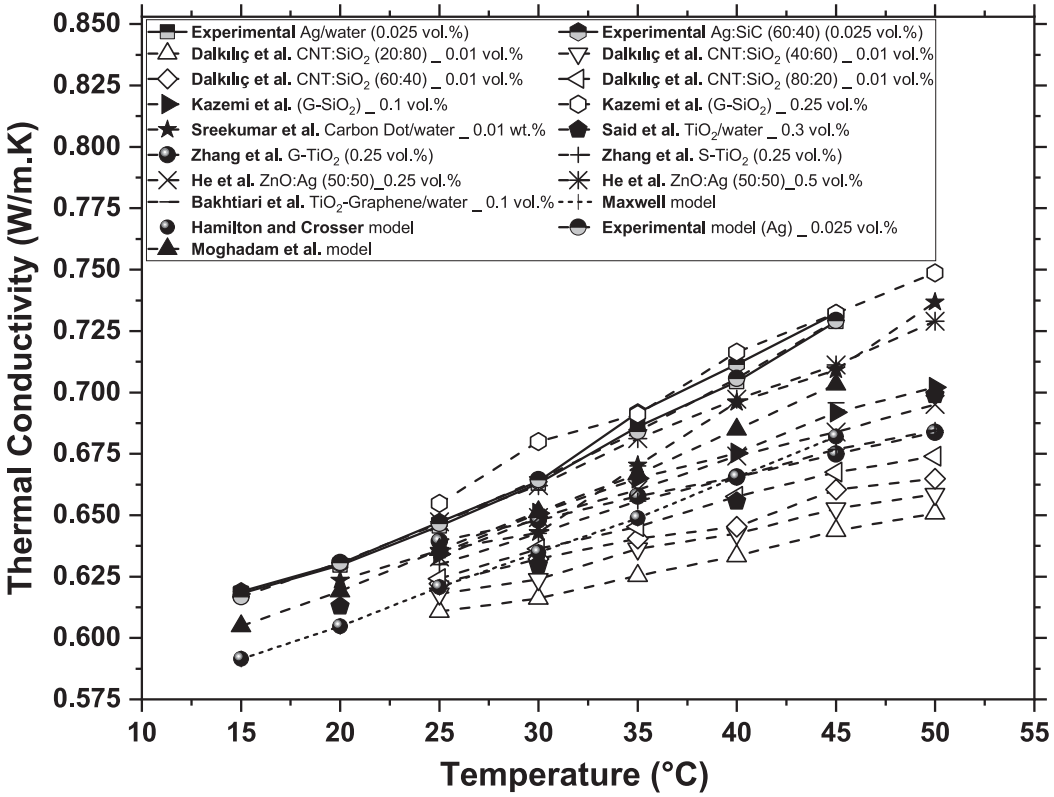

Fig. 18. Comparison of experimental thermal conductivity values with data from literature and theoretical predictions.

0.08 % to 2 vol%, while for surfactant-added TiO_2 (S-TiO_2), it ranged from 2.71 % to 12.67 %. He et al. investigated the thermal conductivity of ZnO-Ag (50 %-50 %)/water hybrid Newtonian nanofluid using Artificial Neural Networks (ANNs) and surface fitting methods. The study found that both methods could predict the nanofluid's behaviour, with the ANN method showing a better ability to predict thermal conductivity based on volume fraction and temperature. It was noted that despite higher concentrations, the thermal conductivity values were lower compared to those obtained in the current study, as ZnO has lower thermal conductivity than SiC and BeO. Moghadam et al. [63] developed a model to predict the thermal conductivity of a graphene oxide-titanium oxide/water hybrid nanofluid. Their results indicated that while the predicted values were close, the model is not recommended for use with other types of nanofluids. This comparative study concluded that no universal model exists for predicting nanofluid thermal conductivity. Models are generally developed for specific fluids and are reliable only if the exact protocols used in the original study are followed.

5.2. Viscosity

Viscosity, a crucial property, requires thorough consideration when examining the characteristics of thermal fluids. To accurately measure the viscosity of prepared samples, we employed the Brookfield DVNext Cone/Plate Rheometer, utilizing a CPA-44PYZ Cup and CPM-40Z cone spindle [64,65]. The spindle rotation speed was set to 100 rpm, and each experiment was allowed to run for 45 s. Ensuring precise temperature control within the testing chamber, the cup was effectively connected to the thermal bath through pipes. Temperature regulation was achieved via a Masterflex L/S Pump, which continuously circulated water throughout the system, maintaining optimal testing conditions. According to the procedural guidelines, a 5 ml sample was utilised for each experiment.

The rheometer used in this study has an accuracy of ± 1.0 % of its full-scale range, ensuring reliable viscosity measurements. The system's reproducibility is within ± 0.2 %, further enhancing the precision of repeated measurements. To validate the test rig, the viscosity of distilled water was examined at different temperatures ranging from 20 °C to 45 °C and compared with the viscosity values of ordinary water available in the literature [66], as shown in Fig. 19. The measured values closely aligned with the literature, with a mean absolute error between the experimental and reference values noted to be 0.59 %. This indicates a high level of accuracy and reliability in the experimental setup.

The study, conducted at 25 °C to investigate the behaviour of the nanofluid samples, revealed that the fluids of Ag, SiC, and BeO behaved as Newtonian fluids, with the shear stress increasing proportionally to

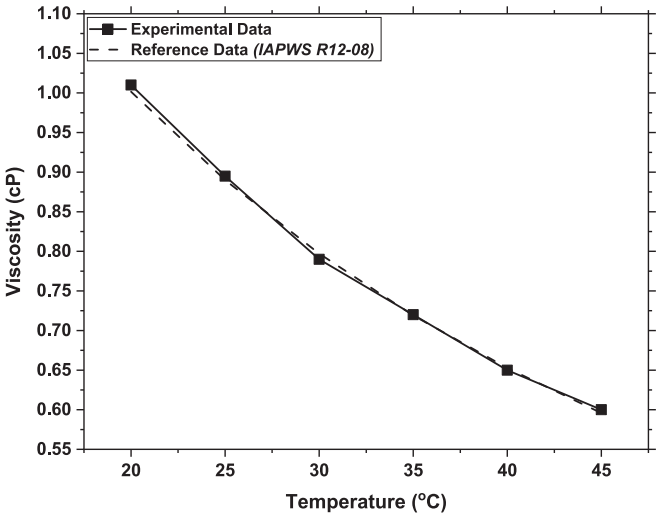

Fig. 19. Comparison of experimental viscosity data for water with reference data from IAPWS R12-08.

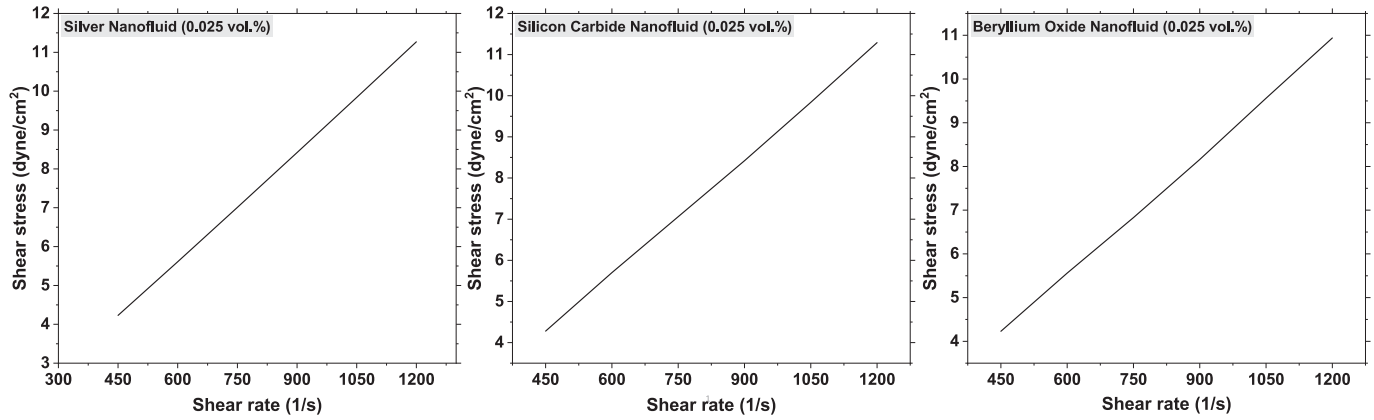

Fig. 20. Shear stress vs shear rate plots for (a) Silver nanofluid, (b) Silicon Carbide nanofluid, and (c) Beryllium Oxide nanofluid at 0.025 vol% concentration, exhibiting Newtonian behaviour.

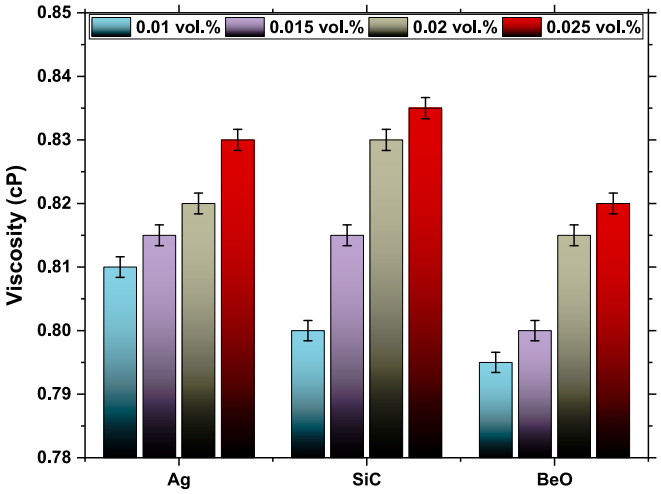

Fig. 21. Viscosity variation at different particle concentrations.

the shear rate. To vary the shear rate, the spindle speed was adjusted in the range of 60 to 160 rpm. This finding suggests that the nanofluids of Ag, SiC, and BeO exhibit Newtonian behaviour, where the relationship between shear stress and shear rate remains linear within the specified range of spindle speeds, as depicted in Fig. 20. Newtonian fluids, with their constant viscosity, are crucial in industrial applications as they ensure stable and predictable flow behaviour under varying shear conditions. This makes them particularly suited for processes such as mixing, pumping, and heat transfer, where precise control over fluid flow is critical. In industries like chemical manufacturing and cooling systems, the reliability of Newtonian fluids simplifies equipment design, improves operational efficiency, and enhances overall system performance.

The concentration study conducted at 30 °C concluded that with the increase in particle concentration, the viscosity of nanofluid increased, as shown in Fig. 21. This is because more particles in the fluid increase the resistance to flow. In the case of the Ag nanofluid, viscosity demonstrated an incremental rise from 0.81 cP to 0.83 cP as nanoparticle concentration escalated from 0.01 vol% to 0.025 vol%. The SiC nanofluid exhibited a proportional increase in viscosity from 0.80 cP to 0.835 cP across the same concentration range. Likewise, the BeO nanofluid experienced a corresponding elevation in viscosity, progressing from 0.795 cP to 0.82 cP.

The results revealed that the silicon carbide nanofluid has the highest viscosity among the three, and attributes this to the fact that the SiC nanoparticles have more sharp edges and irregular shapes. Nanoparticles with sharp edges or irregular shapes can disrupt the flow of the fluid more effectively than nanoparticles with smooth, spherical shapes. It can also be observed in the TEM image of the SiC nanoparticles, which shows that they are indeed more angular and irregular than the other two types of nanoparticles. However, it is important to note that the particle shape is not the only factor which influences the viscosity, factors like particle size, density, etc are also important and need to be considered. Smaller particle size tends to result in higher viscosity due to increased surface area, resulting in more interaction between particles and the fluid [67,68]. The density of nanoparticles also influenced viscosity, with silver nanoparticles exhibiting a density around three times higher than that of SiC and BeO nanoparticles. The combined influence of these factors resulted in the silver nanofluid displaying the highest viscosity, while the BeO nanofluid exhibited comparatively lower viscosity values, as shown in Fig. 22(a). It was also observed that the viscosity values of the nanofluid samples started to converge as the temperature approached 35 °C. This convergence suggests that at higher temperatures and lower particle concentration, the influence of particle type on viscosity becomes less significant especially, resulting in narrowing differences in viscosity among the nanofluid samples.

Fig. 22(b) presents the viscosity values of Ag/BeO-water hybrid nanofluids at different compositions (20/80, 40/60, 60/40, and 80/20) and temperatures ranging from 15 °C to 45 °C. The results revealed that as the percentage of Ag nanofluid increased in the hybrid nanofluid, there was a noticeable improvement in viscosity across all temperatures. It was observed that the viscosity enhancement was more significant with higher proportions of Ag nanoparticles in the hybrid sample. As temperatures approached 35 °C, the disparity in viscosity values among different compositions of the hybrid nanofluid became less pronounced. However, for fluids prepared with higher particle concentrations exceeding 0.1 vol%, the variations in viscosity across different mixing ratios and in comparison to water might remain more pronounced even at elevated temperatures [69].

The viscosity values of Ag and SiC nanofluids are closer to each other, resulting in minor variations in their hybrid fluids' viscosity, as shown in Fig. 22(c). It was noted that the fluid containing a higher percentage of SiC exhibited slightly higher viscosity values, akin to the behaviour

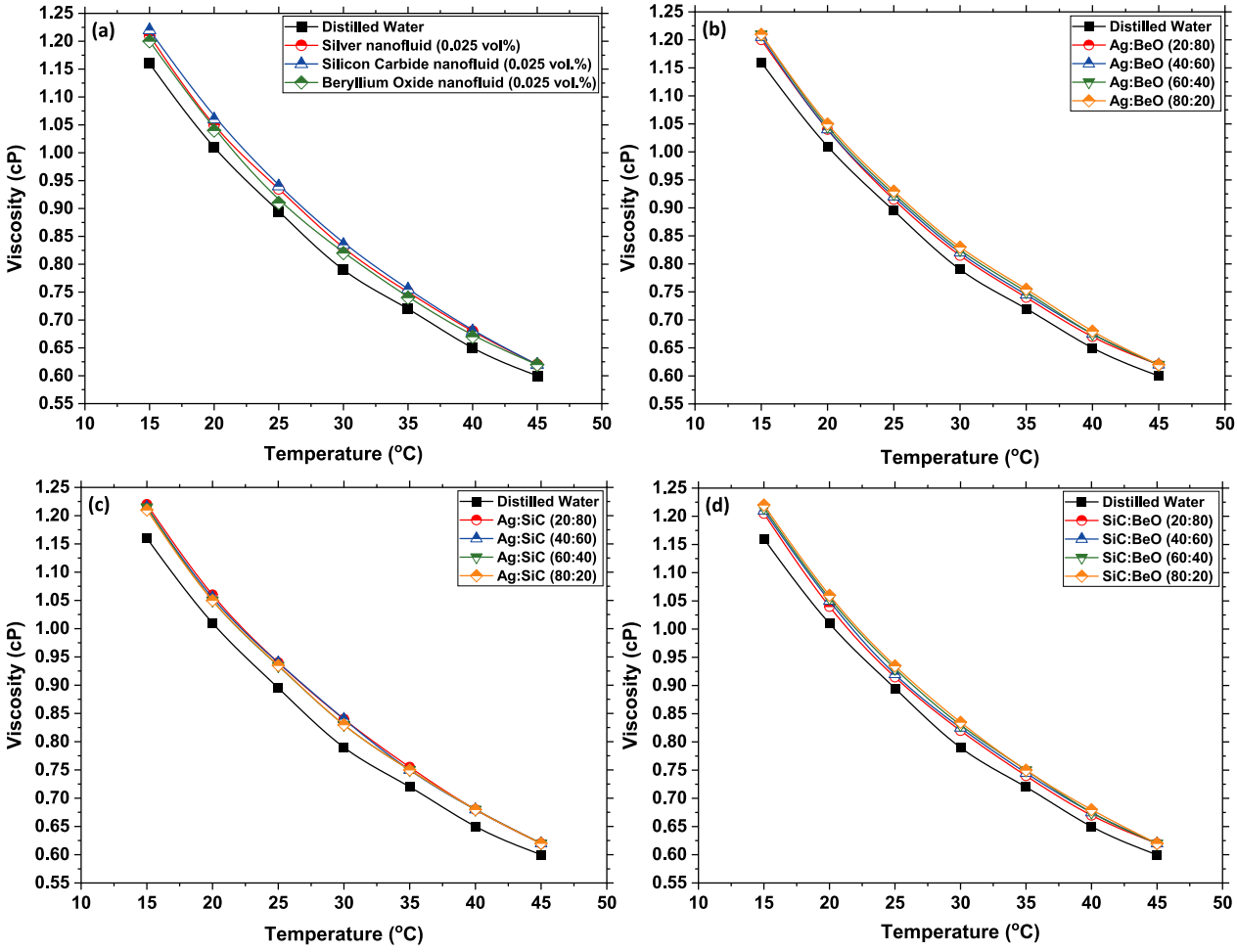

Fig. 22. Viscosity of nanofluid formulations at different temperatures and mixing ratios.

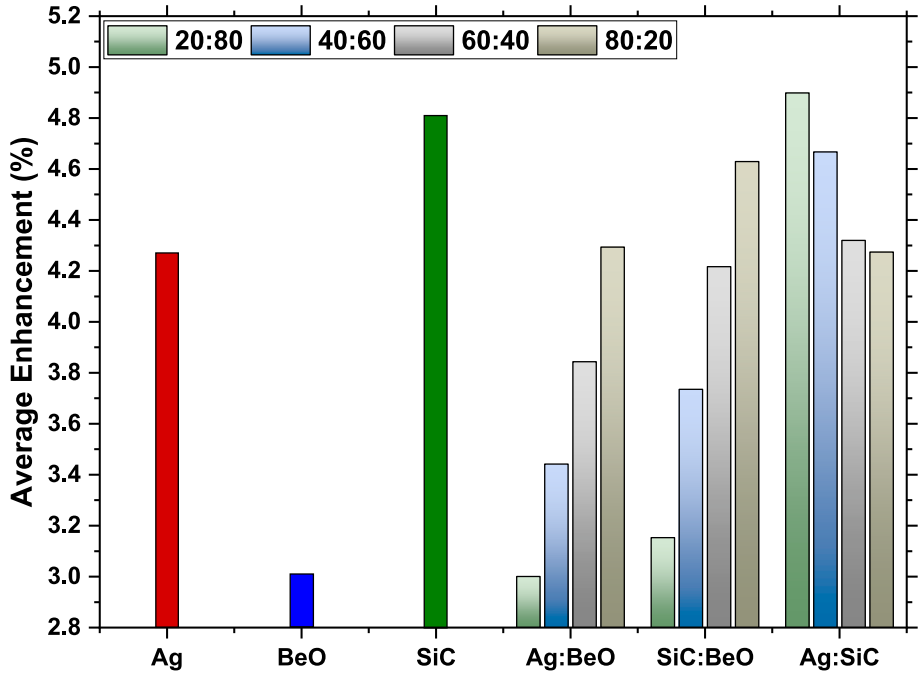

Fig. 23. Average per cent increase in viscosity for different nanofluids and their hybrids compared to basefluid.

Table 4
ANOVA for the cubic model of viscosity.

Source	Sum of Squares	df	Mean Square	F-value	p-value	Significance of model
Model	4.28	48	0.0892	7628.77	< 0.0001	Significant
A-Fluid	0.0106	15	0.0007	60.25	< 0.0001	
B-Temperature	4.14	1	4.14	3.541E + 05	< 0.0001	
AB	0.0010	15	0.0001	5.98	< 0.0001	
B^2	0.1252	1	0.1252	10714.94	< 0.0001	
AB^2	0.0003	15	0.0000	1.97	0.0320	
B^3	0.0037	1	0.0037	316.61	< 0.0001	
Residual	0.0007	63	0.0000			
Std. Dev.	0.00342		**R^2**	0.9998		
Mean	0.8639		**Adjusted R^2**	0.9997		
C.V. %	0.3957		**Predicted R^2**	0.9994		
PRESS	0.0026		**Adeq Precision**	275.2094		

observed in Ag/BeO hybrids, this difference did not manifest significantly at elevated temperatures. The viscosity of SiC/BeO-water hybrid nanofluids exhibited patterns similar to those observed in other hybrid nanofluid samples. Across temperatures ranging from 15 °C to 45 °C, there was a consistent decrease in viscosity across all compositions, which aligns with the typical behaviour of fluids wherein higher temperatures lead to reduced viscosity. However, the viscosity of SiC/BeO nanofluids tended to increase with the percentage of SiC, as illustrated in Fig. 22(d). For instance, at 15 °C, the viscosity of SiC/BeO with a mixing ratio of 80:20 was measured to be 1.205 cP, while for the highest SiC/BeO composition (80/20), it was 1.22 cP, indicating a rise in viscosity with increasing SiC concentration.

When comparing the viscosity enhancements of various simple and hybrid nanofluids to that of water, it is essential to analyse the average per cent increase across different compositions. Fig. 23 provided average per cent increase values that offer valuable insights into the impact of different nanoparticle types and their combinations in altering fluid viscosity. In comparing the viscosity enhancements of various simple and hybrid nanofluids to that of water, it's essential to delve into the nuanced details of their performance. The provided average per cent increase values offer valuable insights into the effectiveness of different nanoparticle types and their combinations in altering fluid viscosity.

For Ag nanofluids, the observed average per cent increase in viscosity stands at approximately 4.27 %. This suggests a moderate enhancement in viscosity when Ag nanoparticles are dispersed within the fluid medium. The SiC nanofluids exhibit a notably higher average per cent increase, at around 4.81 %. This indicates a more significant impact on viscosity, implying that the studied SiC nanoparticles possess a pronounced influence on altering fluid behaviour. Moving on to BeO nanofluids, the average per cent increase is comparatively lower, standing at approximately 3.01 %. The results indicated that BeO nanoparticles had a less substantial effect on viscosity compared to Ag and SiC nanoparticles.

Furthermore, exploring the hybrid nanofluids, both Ag/BeO and SiC/BeO hybrids showcased varying levels of viscosity enhancement across different compositions, Fig. 22. For Ag/BeO hybrids, the average per cent increase ranged from 3.00 % to 4.29 %, with the highest enhancement observed at the 80/20 composition. The SiC/BeO hybrid nanofluids exhibited an average per cent increase ranging from 3.15 % to 4.63 %, with the peak enhancement observed at the 80/20 composition. Finally, Ag/SiC hybrid nanofluids demonstrated moderate to high increases in viscosity across different compositions, with the average per cent increase ranging from 4.27 % to 4.90 %. These samples indicated a notably higher viscosity enhancement compared to the other hybrid fluids.

It is important to note that viscosity is influenced not only by the type of particles present but also by a myriad of other factors like particle shape, size, concentration, and various interparticle interactions. The shape of nanoparticles can significantly impact their ability to interact with the surrounding fluid molecules, thereby affecting viscosity. Similarly, the size of particles plays a crucial role, as smaller nanoparticles tend to exhibit greater surface area-to-volume ratios, potentially leading to stronger interactions with the fluid medium and consequently altering viscosity. Factors like the concentration of nanoparticles within the fluid also play a significant role, with higher concentrations often resulting in more pronounced changes in viscosity. Interactions between particles, like aggregation, further influence nanofluid viscosity. Thus, while particle type is crucial, considering particle characteristics and fluid interactions is vital for understanding viscosity enhancements in nanofluids.

ANOVA analysis was conducted to develop and assess the significance of the cubic model for the viscosity prediction of samples. The model represented with Eq. (3) as a whole exhibits exceptional significance, as indicated by its substantial F-value (7628.77) and minuscule p-value (< 0.0001). Table 4 presents the breakdown of sources of variation, sums of squares, degrees of freedom, mean squares, F-values, and associated p-values. The model's goodness-of-fit was exceptional, as evidenced by the high R^2 value of 0.9998, meaning it explained 99.98 % of the variability in viscosity data. Both the adjusted R^2 (0.9997) and predicted R^2 (0.9994) values were very close to the R^2 value, indicating minimal overfitting and strong predictive performance. Additionally, the adequate precision value of 275.2094, supports the model's effectiveness in exploring the design space. Fig. 24(a) depicts a comparison between experimentally obtained viscosity values and predictions from the cubic model. The close alignment observed suggested that the model accurately predicted viscosity across different experimental conditions, with significant deviations indicating poorer predictive performance. The close alignment of data points with the diagonal line indicates an excellent agreement between experimental data and model predictions. Fig. 24(b) illustrates a normal probability plot of residuals, confirming their adherence to a normal distribution, crucial for ensuring the validity of subsequent statistical analyses. Fig. 24(c) provided a deeper dive into the data by plotting studentized residuals against predicted values. The outcomes showed studentized residuals scattered around zero against predicted values, indicating the model's compliance with assumptions of constant variance and error independence. Furthermore, Fig. 24(d)

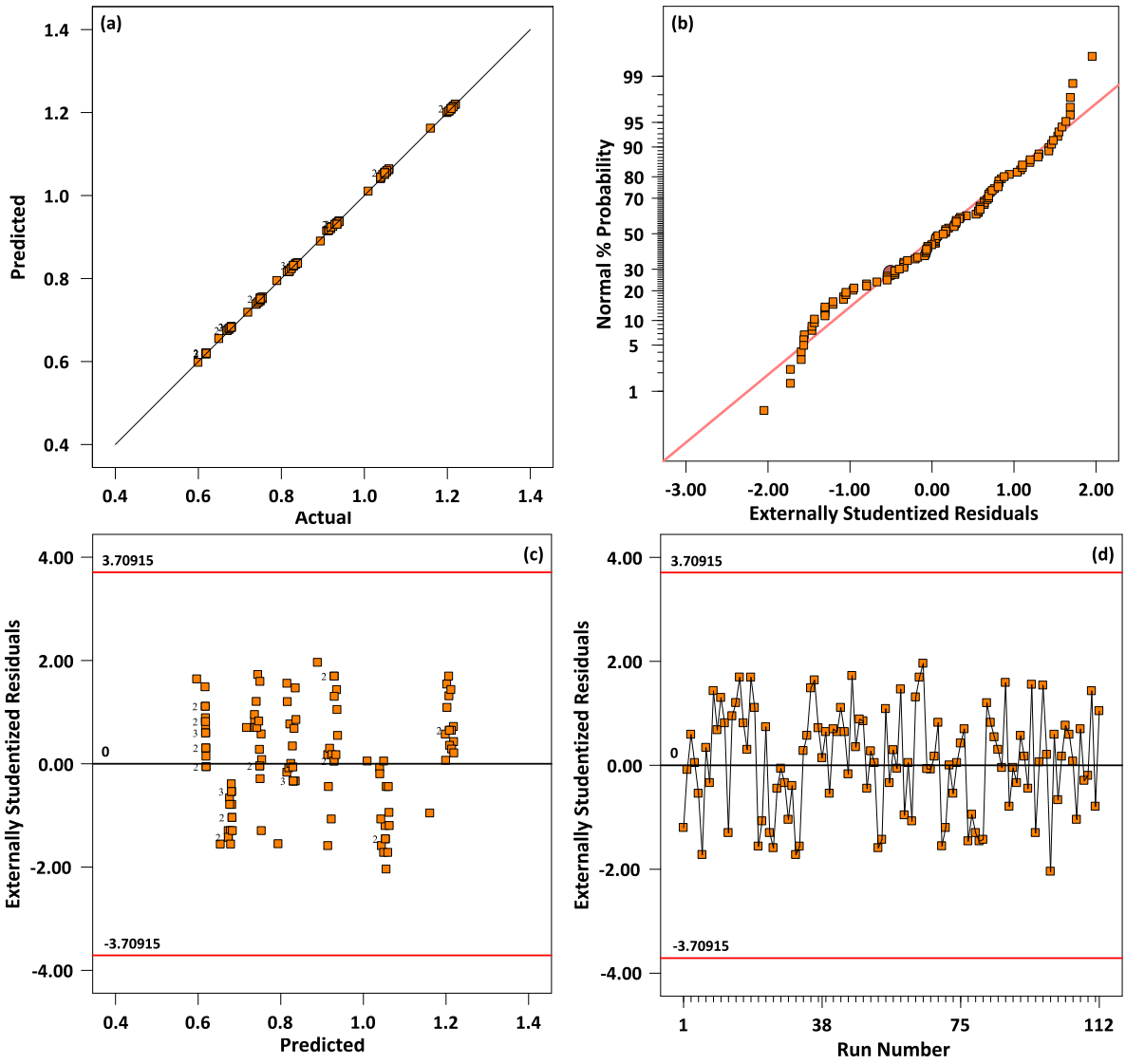

Fig. 24. (a) Comparison of experimental and predicted viscosity values using the developed cubic model, (b) Normal probability plot of studentized residuals for the viscosity model, (c) Plot of studentized residuals vs predicted values for the viscosity model, (d) Plot of externally studentized residuals vs run number for the viscosity model.

Table 5
The values of coefficients for viscosity of fluid samples.

Sample	c	d	e	Sample	c	d	e
DW	1.86683	0.062009	0.001124	SiC/BeO (20:80)	1.94599	0.065116	0.001164
Ag	1.92064	0.062294	0.001114	SiC/BeO (40:60)	1.94683	0.06458	0.001152
SiC	1.93635	0.062651	0.001114	SiC/BeO (60:40)	1.9423	0.063651	0.001133
BeO	1.93647	0.064687	0.001159	SiC/BeO (80:20)	1.94635	0.063509	0.001128
Ag/BeO (20:80)	1.93945	0.064866	0.001162	Ag/SiC (20:80)	1.92945	0.06208	0.001105
Ag/BeO (40:60)	1.93457	0.064187	0.00115	Ag/SiC (40:60)	1.91921	0.061651	0.0011
Ag/BeO (60:40)	1.93397	0.063651	0.001138	Ag/SiC (60:40)	1.93487	0.063194	0.001127
Ag/BeO (80:20)	1.91849	0.062223	0.001114	Ag/SiC (80:20)	1.92064	0.062294	0.001114

validates model assumptions, showing externally studentized residuals randomly distributed across observation numbers, mitigating concerns about biases related to experimental order. Together, these graphical analyses confirm the quadratic model's robustness and the data's compliance with fundamental statistical assumptions.

$$Viscosity(\mu) = c - dT + e(T^2) - 8.2778 \times 10^{-6}(T^3) \quad (3)$$

here c, d, and e are coefficients that vary for each specific nanofluid sample as listed in Table 5.

5.3. Density

Density is a critical thermo-physical property to investigate, especially concerning its impact on enhancing pumping power and mass flow rate in various application areas. The density of both basefluid and nanofluid samples was measured using an Anton Paar DMA 35 density meter at different temperatures [70,71]. To achieve the desired

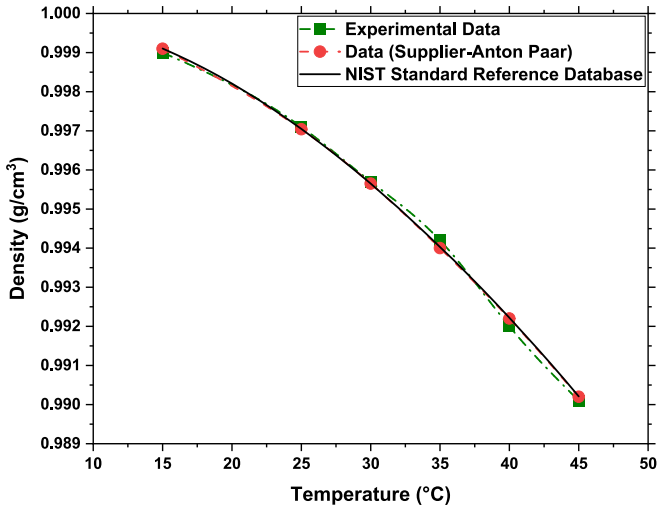

Fig. 25. Validation of experimental density data against reference values for water.

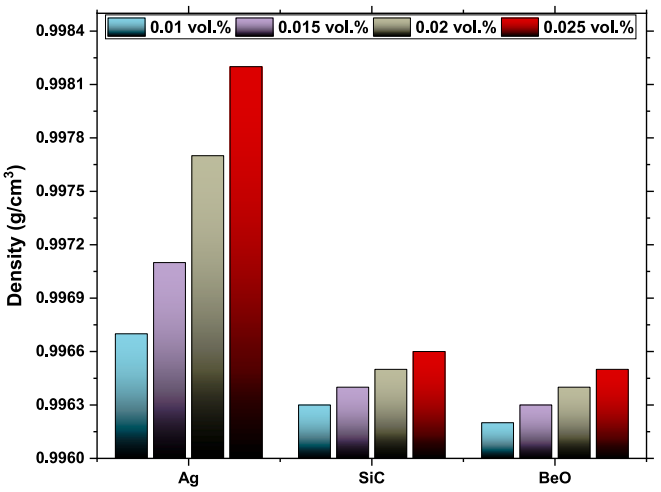

Fig. 26. Variation of density with nanoparticle concentration at 30 °C for Ag, SiC, and BeO nanofluids.

temperature, the samples were poured into a sample tube immersed in a temperature-controlled bath. After allowing sufficient time for temperature stabilization, measurements were taken following a specific set of instructions. Prior to conducting the measurements and validation study, a water check was performed according to the supplier's instructions. The density meter used in this study has an accuracy of ± 0.001 g/cm3 for density and ± 0.2 °C for temperature. The system's repeatability is excellent, with a standard deviation of ± 0.0005 g/cm3 for density and ± 0.1 °C for temperature. To ensure precision, three measurements were taken at each temperature point, and the average was reported. The transparent glass top of the chamber facilitates ensuring the absence of air bubbles in the measurement section of the U-tube. For validation purposes, the density of water was measured over a temperature range of 15 – 45 °C and compared with values provided by the supplier and those available in the literature [72], Fig. 25. The obtained data closely matched the literature and supplier values, with a mean absolute error of 0.02 %.

A study was conducted by analysing the density of studied nanofluids by varying particle concentrations at 30 °C. The results revealed a noticeable enhancement in density values with changing particle concentration, attributed to the higher particle density compared to the base fluid. Among the nanofluids tested, silver nanofluid exhibited the most significant density increase, reaching a value of 0.9982 g/cm^3 at a concentration of 0.025 vol%, which represents a 0.2410 % enhancement compared to the base fluid. As depicted in Fig. 26, a consistent pattern was observed as the concentration increased from 0.01 to 0.025 vol% across all three types of nanofluids while the Ag nanofluid consistently displayed the highest density enhancement, followed by SiC and BeO nanofluids, respectively.

The density of SiC nanofluids ranged from 0.9963 g/cm^3 to 0.9966 g/cm^3 as the particle concentration varied from 0.01 to 0.025 vol%. The enhancement in density varied from 0.0502 % to 0.08033 % across these concentration levels. The beryllium oxide nanofluids displayed the least enhancement in density throughout all concentrations tested. At the maximum concentration of 0.025 vol%, the fluid only reached a density of 0.9982 g/cm^3, which is a 0.07029 % increase from the base fluid.

The density of simple and hybrid nanofluid samples was examined at various temperatures ranging from 15 °C to 45 °C. It was observed that as the temperature increased, the density values decreased significantly. This trend aligns with the expected behaviour, as higher temperatures typically lead to reduced fluid densities due to thermal expansion effects. However, the extent of the decrease varies slightly depending on the presence of nanoparticles. At 15 °C, water exhibited a density of 0.9990 g/cm^3, which decreased to 0.9901 g/cm^3 at 45 °C, indicating a notable reduction in density with increasing temperature. Similar trends were observed for other simple and hybrid nanofluid samples examined, as shown in Fig. 27. The density of Ag nanofluid is comparatively higher than that of water, with a value of 1.00195 g/cm^3 compared to 0.9990 g/cm^3 for water. Despite the decrease in density with temperature, Ag nanofluid maintained a slightly higher density compared to water and other unitary nanofluid samples throughout the temperature range. At 45 °C, the density of Ag nanofluid was noted to be 0.9926 g/cm^3, while the density of water was 0.9901 g/cm^3.

The density of SiC at the lower end of the temperature range was recorded to be 1.0 g/cm^3. With increasing temperature, a consistent decrease in density was observed. At the upper end of the range, at 45 °C, the density had decreased to 0.9911 g/cm^3. In comparison to water and BeO nanofluid, SiC exhibited a higher density but lower than that of Ag nanofluid. BeO nanofluid demonstrated a decreasing density trend from 0.9998 at 15 °C to 0.9909 at 45 °C, mirroring trends seen in water, Ag, and SiC nanofluids. Comparatively, its densities were slightly higher than water but lower than Ag and SiC nanofluids over the temperature range.

Fig. 27(b) presents the density values for the hybrid nanofluids of Ag/BeO with mixing ratios of 20/80, 40/60, 60/40, and 80/20 across various temperatures. Upon analysing the hybrid nanofluid densities, it was observed that the mixing ratios significantly influenced the resulting densities. As the proportion of Ag increased relative to BeO (20/80 to 80/20), there was a discernible trend of increasing density across all temperature points. For instance, at 15 °C, the density of the hybrid nanofluid with a mixing ratio of 20/80 (Ag/BeO) was 1.0003 g/cm^3, gradually increasing to 1.0014 g/cm^3 for the 80/20 mixing ratio. This indicated that increasing the proportion of Ag in the hybrid nanofluid led to higher overall densities. Similarly, this trend persisted across all temperature points, with the densities of hybrid nanofluids at the 80/20 mixing ratio consistently surpassing those at the 20/80 mixing ratio.

As anticipated, the density of SiC/BeO hybrid nanofluids consistently decreased with rising temperature. However, slight differences in values

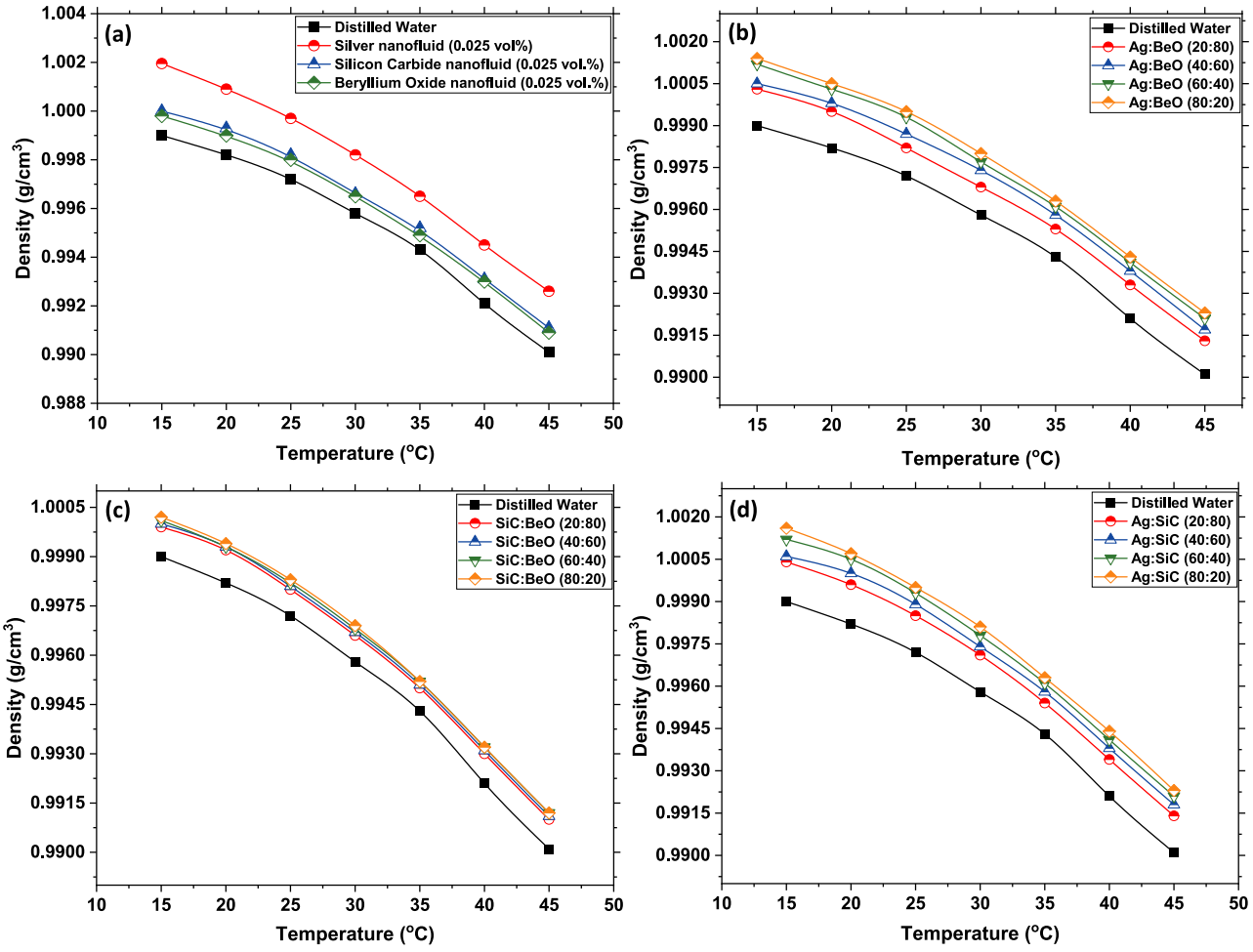

Fig. 27. Temperature dependence of density for simple and hybrid nanofluid samples.

were observed as the mixing ratio changed, attributed to the slight disparity in the individual densities of SiC and BeO nanoparticles, as depicted in Fig. 27(c). The results suggest that the density is more influenced by temperature than the specific mixing ratio of SiC and BeO nanoparticles. At 15 °C, the density of SiC/BeO hybrid nanofluid samples ranged from approximately 0.9999 g/cm^3 to 1.0002 g/cm^3, while at 45 °C, it decreased to approximately 0.9910 g/cm^3 to 0.9912 g/cm^3 across all mixing ratios.

The density of Ag/SiC nanofluid, when compared to other hybrid nanofluids, generally exhibited higher values across all mixing ratios and temperature points, Fig. 27(d). However, there existed only a minor difference between the densities of Ag/SiC and Ag/BeO nanofluids. Across different mixing ratios, the density of Ag/SiC hybrid nanofluids displayed slight variations, showing an increase in values as the ratio of Ag in the mixture increased. The average percentage increase for nanofluids and their hybrids presented in Fig. 28, offers valuable insights into the density rise across various mixing ratios. It is evident that the inclusion of silver nanoparticles notably enhanced the density values, whereas the density variation in SiC/BeO nanofluid was comparatively less significant due to the close density values of the particles themselves.

The results suggested that temperature, the choice of nanoparticles, and mixing ratio for the case of hybrid nanofluids significantly influenced the density, and understanding these variations was crucial for optimising the properties for specific applications.

As part of this study, an analysis was performed using Design Expert and a cubic model was developed to predict density based on temperature variations in various nanofluids, Eq. (4). ANOVA analysis

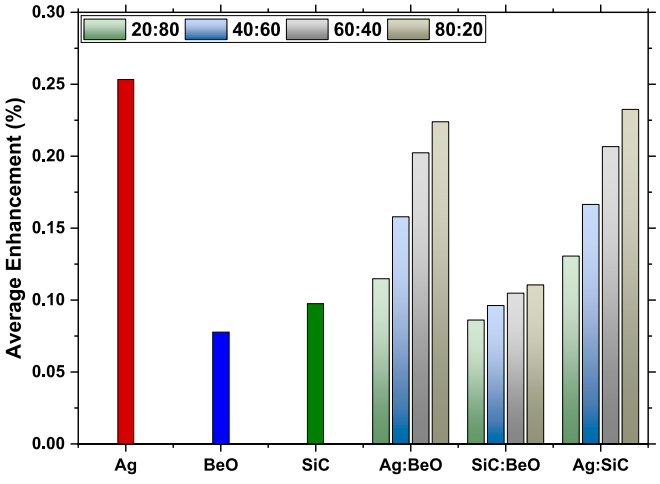

Fig. 28. Average percentage enhancement in density for various nanofluids and their hybrids compared to the base fluid.

confirmed the model's overall significance ($p < 0.0001$) and the statistical significance of its terms, as presented in Table 6. The model's Std. Dev. was calculated to be 0.0001, with an R^2 of 0.9998, indicating its ability to explain 99.98 % of density variability. Predicted R^2 (0.9992) is closely aligned with Adjusted R^2 (0.9996), demonstrating consistent predictive power. The C.V. was 0.0065 %, and the PRESS value was 8.95E-07, indicating precise predictions.

Table 6
ANOVA for the cubic model of Density.

Source	Sum of Squares	df	Mean Square	F-value	p-value	Significance of model
Model	0.0011	48	0	5416.8	< 0.0001	Significant
A-Fluid	0	15	3.27E-06	771.68	< 0.0001	
B-Temperature	0.001	1	0.001	2.43E + 05	< 0.0001	
AB	3.01E-07	15	2.00E-08	4.73	< 0.0001	
B^2	0	1	0	5325.12	< 0.0001	
AB^2	1.31E-07	15	8.73E-09	2.06	0.0242	
B^3	1.88E-07	1	1.88E-07	44.4	< 0.0001	
Residual	2.67E-07	63	4.24E-09			
Std. Dev.	0.0001		**R^2**	0.9998		
Mean	0.9966		**Adjusted R^2**	0.9996		
C.V. %	0.0065		**Predicted R^2**	0.9992		
PRESS	8.95E-07		**Adeq Precision**	275.037		

Table 7
Coefficients values for the density of various fluid samples.

Sample	f	g	h	Sample	f	g	h
DW	0.998269	0.000199	0.000011	SiC/BeO (20:80)	0.999685	0.00016	0.000011
Ag	1.00262	0.000082	9.43E-06	SiC/BeO (40:60)	0.999785	0.00016	0.000011
SiC	0.999723	0.000165	0.000011	SiC/BeO (60:40)	0.999828	0.000161	0.000011
BeO	0.999421	0.00017	0.000011	SiC/BeO (80:20)	0.999938	0.000163	0.000011
Ag/BeO (20:80)	1.00047	0.000124	9.93E-06	Ag/SiC (20:80)	1.00014	0.000163	0.000011
Ag/BeO (40:60)	0.999771	0.0002	0.000011	Ag/SiC (40:60)	1.00014	0.000184	0.000011
Ag/BeO (60:40)	1.00117	0.000143	0.00001	Ag/SiC (60:40)	1.00114	0.000151	0.000011
Ag/BeO (80:20)	1.00123	0.000154	0.000011	Ag/SiC (80:20)	1.00171	0.000131	0.00001

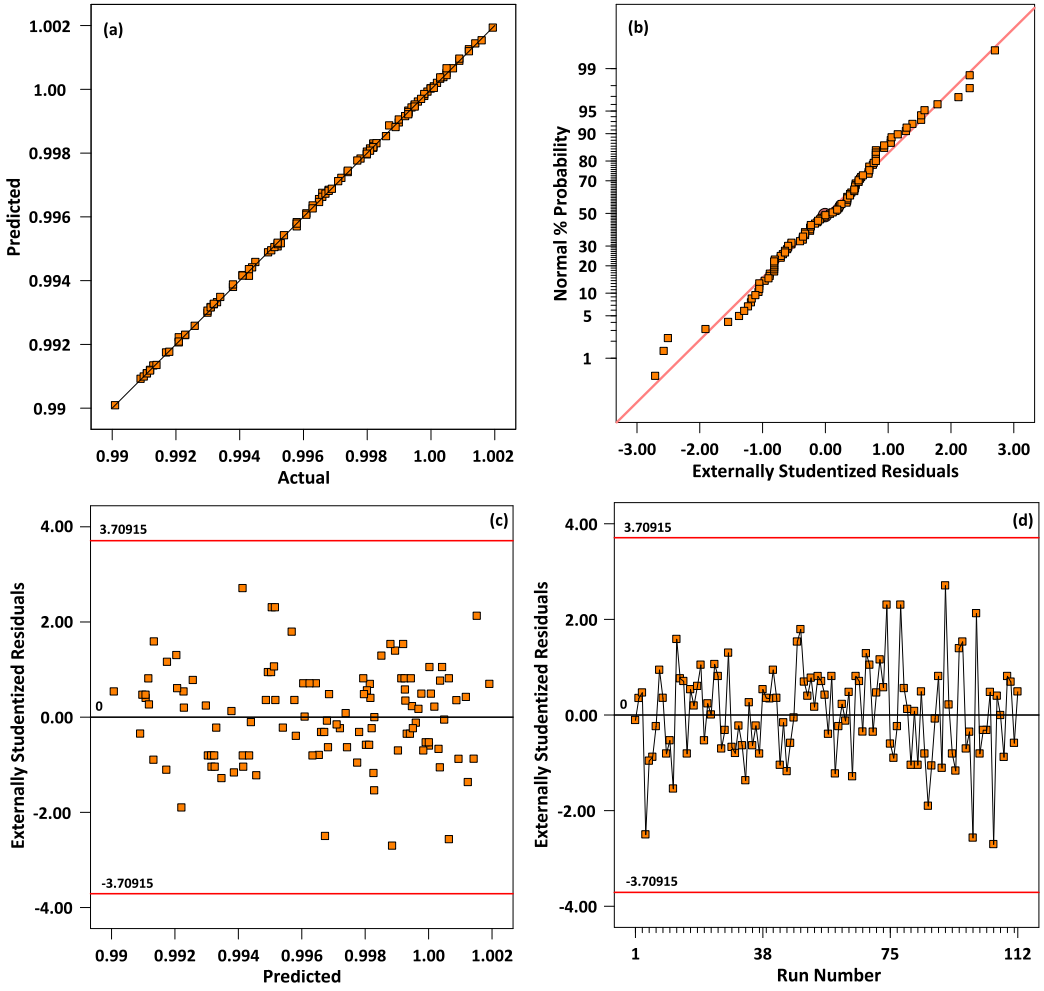

Fig. 29. (a) Parity plot comparing experimental and predicted density values using the developed cubic model, (b) Normal probability plot of studentized residuals for the density model, (c) Residuals vs predicted values plot for the density model, (d) Externally studentized residuals vs run order plot for the density model.

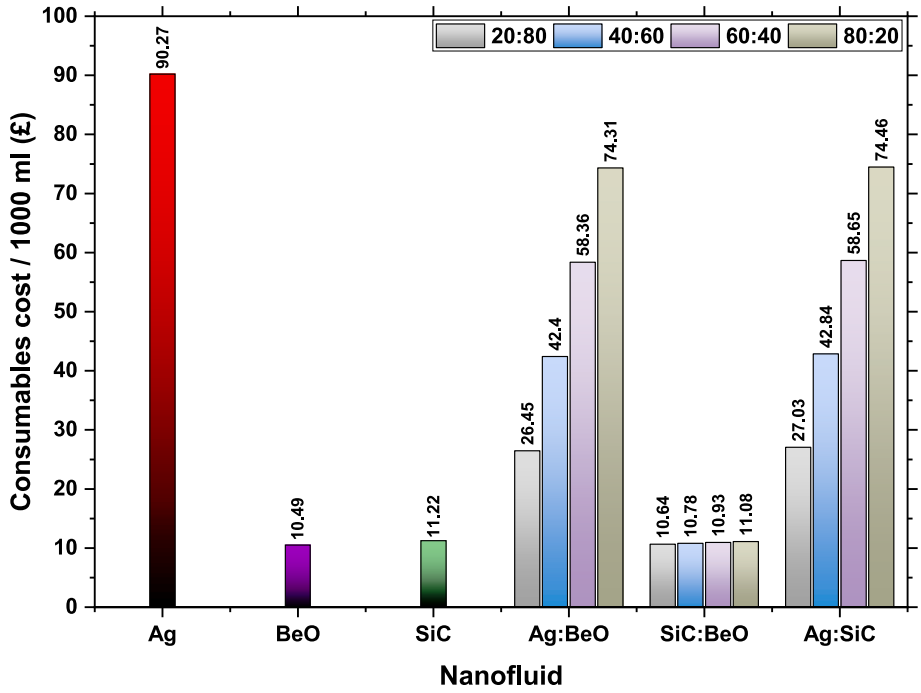

Fig. 30. Consumables cost per 1000 ml of different nanofluids and their hybrids.

$$Density(\rho) = f + gT - h(T^2) + 5.90278 \times 10^{-8}(T^3) \quad (4)$$

here f, g, and h denote coefficients representing the intercept, linear coefficient, and quadratic effect of temperature, respectively. Specific values for these coefficients are assigned to each nanofluid sample, as listed in Table 7.

The comparison between experimental and predicted density values using the ANOVA model revealed a satisfactory fit, with the alignment of points with the diagonal line in Fig. 29(a). Additionally, the normal probability plot of studentized residuals, depicted in Fig. 29(b), confirmed the normal distribution of errors associated with density values. Residual plots, shown in Fig. 29(c) and Fig. 29(d), assist in assessing covariance among errors related to independent variables. In this case, no discernible patterns or structures were observed, indicating the presence of covariance among errors.

6. Cost analysis

The cost analysis was conducted to provide insights to investigators and manufacturers regarding the expenses associated with the preparation of various nanofluids and their hybrids. The evaluation takes into account the costs of nanoparticles, surfactants, and base fluid, excluding the costs related to electricity usage during operations such as sonication, stirring, and ultrasonication, as these are consistent across all samples. Moreover, laboratory resource utilization costs were not factored into this analysis.

The results of the cost analysis are depicted in Fig. 30, which illustrates the costs of preparing 1000 ml for various samples. Among all the studied fluids, silver nanofluid is the most expensive to prepare due to its particle price, while beryllium oxide and silicon carbide nanofluids are comparatively much cheaper to prepare. This is one of the major reasons why hybrid nanofluids are gaining more attention from the scientific community. The cost difference between beryllium oxide and silicon carbide nanofluids is minimal, although the silicon carbide nanofluid demonstrated better stability.

Hybrid nanofluids exhibited varying costs based on mixing ratios. The cost range for hybrid nanofluids of Ag-SiC and Ag-BeO varies between 25 and 75 lb. However, SiC-BeO hybrid combinations fall within the range of 10.5 to 11.1 lb across all mixing ratios from 20:80 to 80:20. Notably, the choice of hybrid nanofluid is not solely based on cost, it also considers thermal and rheological characteristics. The results suggest that the Ag-SiC hybrid nanofluid, particularly with a 60:40 mixing ratio stands out as a good balance of characteristics and cost. The 20:80 and 40:60 ratios are less expensive, while the 80:20 ratio is the most expensive among the Ag-SiC combinations.

The cost analysis reveals that silver nanofluid is the most expensive among the studied fluids. However, the hybrid combinations, such as Ag-SiC and Ag-BeO, exhibit a more favourable cost range. This makes hybrid nanofluids an attractive option for those seeking cost-efficient thermal solutions.

7. Conclusion

This study thoroughly examined the thermophysical properties of nanofluids containing silver Ag, BeO, and SiC nanoparticles, with a particular emphasis on hybrid formulations. The results revealed significant improvements in thermal conductivity, viscosity, and density for pure and hybrid nanofluids compared to the base fluid, water. These findings underscore the potential of hybrid nanofluids to advance thermal management systems, offering a promising approach to improving heat transfer efficiency while addressing stability and cost issues. The key outcomes of this study are:

- The addition of surfactants played a crucial role in stabilising nanofluids and altering their pH values. The anionic surfactant SDBS demonstrated superior stability for all three nanofluids (silver, beryllium oxide, and silicon carbide) and consistently increased the pH values toward neutrality. At a particle concentration of 0.01 vol %, the pH values were recorded as 7.2 for Ag, 7.08 for BeO, and 7.45 for SiC, with pH increasing as concentration rose to 0.025 vol%.
- Hybrid nanofluid formulations prepared with different ratios exhibited varying pH trends. The Ag/BeO hybrid showed an increase in pH from 7.25 (20/80) to 7.33 (80/20) with higher Ag concentration, while the SiC/BeO hybrid exhibited a consistent rise from 7.36 (20/80) to 7.59 (80/20) with increasing SiC proportion.

Conversely, the Ag/SiC hybrid displayed a decrease in pH from 7.62 (20/80) to 7.41 (80/20) with higher Ag concentration.

- Larger particle sizes, as observed for BeO nanofluid, led to earlier sedimentation and reduced long-term stability despite high zeta potential, while smaller Ag and SiC nanoparticles exhibited better dispersion due to less gravitational settling and aggregation.
- Hybrid nanofluids exhibited smaller agglomerate sizes (192–271 nm) compared to unitary Ag (218.4 nm), BeO (404.3 nm), and SiC (230.9 nm) nanofluids, indicating reduced agglomeration tendency due to the presence of different nanoparticles and uneven attractive forces in the hybrid suspension. Notably, SiC nanoparticles demonstrated a unique tendency to form agglomerates in the form of chains, with connections between particles appearing weaker compared to those observed in Ag and BeO nanoparticles.
- The thermal conductivity of the simple nanofluids increased with increasing particle concentration from 0.01 vol% to 0.025 vol%, with the silver nanofluid exhibiting the highest thermal conductivity enhancement of 6.95 % at 0.025 vol% and 45 °C. Hybrid nanofluids also outperformed water, with the Ag/SiC (60/40) formulation demonstrating the maximum enhancement of 7.43 % at 45 °C.
- Nanofluids exhibited Newtonian behaviour, characterized by a linear relationship between shear stress and shear rate. Additionally, the viscosity of these nanofluids increased with nanoparticle concentrations due to increased internal resistance to flow. SiC nanoparticles, which had a more irregular shape and sharp edges, exhibited the highest viscosity among the unitary nanofluids, likely due to their ability to disrupt fluid flow more effectively.
- Among the hybrid nanofluids, Ag/SiC exhibited the highest average viscosity enhancement, ranging from 4.27 % to 4.90 % across different mixing ratios. The Ag/BeO hybrids showed a 3.00 % to 4.29 % increase, while SiC/BeO hybrids demonstrated a 3.15 % to 4.63 % enhancement compared to the base fluid. The extent of viscosity increase was influenced by the mixing ratio and the type of nanoparticles present.
- Silver nanofluids exhibited the most substantial increase in density, with the enhancement becoming more pronounced as particle loading increased. In the case of hybrid Ag/BeO nanofluids, the density increased with higher Ag ratios. However, Ag/SiC hybrid nanofluids generally exhibited the highest density values among all hybrid formulations, with the 80/20 Ag/SiC ratio reaching 1.0016 g/cm^3 at 15 °C.
- Advanced statistical analyses, including ANOVA, yielded highly accurate models for predicting nanofluid thermal conductivity, viscosity, and density, with strong R^2 values and close alignment between experimental and predicted results.
- The cost analysis revealed that silver Ag nanofluid is the most expensive option among the studied nanofluids, with a cost of £90.27 per 1000 ml, due to the high cost of silver nanoparticles. Hybrid nanofluids, like Ag-SiC and Ag-BeO, cost between £25 and £75 per 1000 ml, offering a more economical alternative to pure silver nanofluid while potentially providing favourable thermal and rheological properties.

The study highlights the potential of hybrid nanofluids to revolutionize thermal management systems by offering a balanced trade-off between improved thermophysical properties and economic considerations. The Ag-SiC (60:40) hybrid nanofluid, in particular, emerged as a promising candidate, balancing performance and cost. Future research should focus on the long-term stability of these nanofluids and their practical applications in various industries to fully harness their potential in enhancing heat transfer efficiency and addressing energy challenges.

CRediT authorship contribution statement

Hamza Babar: Writing – review & editing, Writing – original draft, Visualization, Validation, Methodology, Investigation, Formal analysis, Data curation, Conceptualization. **Hongwei Wu:** Writing – review & editing, Supervision, Funding acquisition, Conceptualization. **Wenbin Zhang:** Writing – review & editing, Supervision, Conceptualization. **Yongqi Xie:** Supervision, Conceptualization.

Declaration of competing interest

The authors declare that they have no known competing financial interests or personal relationships that could have appeared to influence the work reported in this paper.

Data availability

Data will be made available on request.

Acknowledgement

The authors gratefully acknowledge the financial support from the Engineering and Physical Sciences Research Council (EPSRC), United Kingdom (Grant No. EP/X038319/1). This support was provided under the framework of the Horizon Europe project Marie Skłodowska-Curie Actions (MSCA), with Grant No. 101082394.

References

[1] S. Jana, A. Salehi-Khojin, W.-H. Zhong, Enhancement of fluid thermal conductivity by the addition of single and hybrid nano-additives, Thermochim. Acta. 462 (2007) 45–55, https://doi.org/10.1016/j.tca.2007.06.009.
[2] H. Babar, H. Wu, W. Zhang, T.R. Shah, D. McCluskey, C. Zhou, The promise of nanofluids: a bibliometric journey through advanced heat transfer fluids in heat exchanger tubes, Adv. Colloid Interface Sci. 325 (2024) 103112, https://doi.org/10.1016/j.cis.2024.103112.
[3] M. Sheikholeslami, Z. Khalili, Simulation for impact of nanofluid spectral splitter on efficiency of concentrated solar photovoltaic thermal system, Sustain. Cities Soc. 101 (2024) 105139, https://doi.org/10.1016/j.scs.2023.105139.
[4] M.A. Khairul, K. Shah, E. Doroodchi, R. Azizian, B. Moghtaderi, Effects of surfactant on stability and thermo-physical properties of metal oxide nanofluids, Int. J. Heat Mass Transf. 98 (2016) 778–787, https://doi.org/10.1016/j.ijheatmasstransfer.2016.03.079.
[5] M. Ma, Y. Zhai, P. Yao, Y. Li, H. Wang, Effect of surfactant on the rheological behavior and thermophysical properties of hybrid nanofluids, Powder Technol. 379 (2021) 373–383, https://doi.org/10.1016/j.powtec.2020.10.089.
[6] P.K. Kanti, P. Sharma, M.P. Maiya, K.V. Sharma, The stability and thermophysical properties of Al2O3-graphene oxide hybrid nanofluids for solar energy applications: application of robust autoregressive modern machine learning technique, Sol. Energy Mater. Sol. Cells 253 (2023) 112207, https://doi.org/10.1016/j.solmat.2023.112207.
[7] A. Ghadimi, I.H. Metselaar, The influence of surfactant and ultrasonic processing on improvement of stability, thermal conductivity and viscosity of titania nanofluid, Exp. Therm Fluid Sci. 51 (2013) 1–9, https://doi.org/10.1016/j.expthermflusci.2013.06.001.
[8] F. Li, L. Li, G. Zhong, Y. Zhai, Z. Li, Effects of ultrasonic time, size of aggregates and temperature on the stability and viscosity of Cu-ethylene glycol (EG) nanofluids, Int. J. Heat Mass Transf. 129 (2019) 278–286, https://doi.org/10.1016/j.ijheatmasstransfer.2018.09.104.
[9] H. Guan, Q. Su, R. Wang, L. Huang, C. Shao, Z. Zhu, Why can hybrid nanofluid improve thermal conductivity more? A Molecular Dynamics Simulation, J Mol Liq 372 (2023) 121178 https://doi.org/10.1016/j.molliq.2022.121178.
[10] E.M. Cárdenas Contreras, G.A. Oliveira, E.P. Bandarra Filho, Experimental analysis of the thermohydraulic performance of graphene and silver nanofluids in automotive cooling systems, Int J Heat Mass Transf 132 (2019) 375–387, https://doi.org/10.1016/j.ijheatmasstransfer.2018.12.014.
[11] K.V. Sharma, P.H.V.S. Talpa Sai, P. Sharma, P.K. Kanti, P. Bhramara, S. Akilu, Prognostic modeling of polydisperse SiO2/Aqueous glycerol nanofluids' thermophysical profile using an explainable artificial intelligence (XAI) approach, Eng. Appl. Artif. Intell. 126 (2023) 106967, https://doi.org/10.1016/j.engappai.2023.106967.
[12] P. Kanti, K.V. Sharma, R.S. Khedkar, T. Rehman, Synthesis, characterization, stability, and thermal properties of graphene oxide based hybrid nanofluids for

thermal applications: Experimental approach, Diam. Relat. Mater. 128 (2022) 109265, https://doi.org/10.1016/j.diamond.2022.109265.
[13] M. Hemmat Esfe, S. Saedodin, M. Biglari, H. Rostamian, An experimental study on thermophysical properties and heat transfer characteristics of low volume concentrations of Ag-water nanofluid, in: International Communications in Heat and Mass Transfer 74, 2016, pp. 91–97, https://doi.org/10.1016/j.icheatmasstransfer.2016.03.004.
[14] B.C. Pak, Y.I. Cho, Hydrodynamic and heat transfer study of dispersed fluids with submicron metallic oxide particles, Exp. Heat Transfer 11 (1998) 151–170, https://doi.org/10.1080/08916159808946559.
[15] Y. Xuan, W. Roetzel, Conceptions for heat transfer correlation of nanofluids, Int. J. Heat Mass Transf. 43 (2000) 3701–3707, https://doi.org/10.1016/S0017-9310(99)00369-5.
[16] H. Chen, Y. Zhang, L. Huang, X. Zhao, X. Ma, Z. Ma, J. Hou, J. Wei, P. Di Marco, O. Mahian, N. Hao, Microfluidic production of silica nanofluids for highly efficient two-phase cooling with micro pin-fins structure, Chem. Eng. J. 465 (2023) 142799, https://doi.org/10.1016/j.cej.2023.142799.
[17] H. Maddah, M. Rezazadeh, M. Maghsoudi, S. NasiriKokhdan, The effect of silver and aluminum oxide nanoparticles on thermophysical properties of nanofluids, J. Nanostruct. Chem. 3 (2013) 28, https://doi.org/10.1186/2193-8865-3-28.
[18] G. Huminic, A. Huminic, C. Fleaca, F. Dumitrache, I. Morjan, Thermo-physical properties of water based SiC nanofluids for heat transfer applications, Int. Commun. Heat Mass Transfer 84 (2017) 94–101, https://doi.org/10.1016/j.icheatmasstransfer.2017.04.006.
[19] Q. Luo, C. Wang, H. Wen, L. Liu, Research and optimization of thermophysical properties of sic oil-based nanofluids for data center immersion cooling, Int. Commun. Heat Mass Transfer 131 (2022) 105863, https://doi.org/10.1016/j.icheatmasstransfer.2021.105863.
[20] M. Sheikholeslami, Z. Khalili, Solar photovoltaic-thermal system with novel design of tube containing eco-friendly nanofluid, Renew. Energy 222 (2024) 119862, https://doi.org/10.1016/j.renene.2023.119862.
[21] M. Sheikholeslami, Z. Khalili, P. Scardi, N. Ataollahi, Environmental and energy assessment of photovoltaic-thermal system combined with a reflector supported by nanofluid filter and a sustainable thermoelectric generator, J. Clean. Prod. 438 (2024) 140659, https://doi.org/10.1016/j.jclepro.2024.140659.
[22] M. Abbasi, M.M. Heyhat, A. Rajabpour, Study of the effects of particle shape and base fluid type on density of nanofluids using ternary mixture formula: a molecular dynamics simulation, J. Mol. Liq. 305 (2020) 112831, https://doi.org/10.1016/j.molliq.2020.112831.
[23] S. Nabati Shoghl, J. Jamali, M. Keshavarz Moraveji, Electrical conductivity, viscosity, and density of different nanofluids: An experimental study, Exp. Therm Fluid Sci. 74 (2016) 339–346, https://doi.org/10.1016/j.expthermflusci.2016.01.004.
[24] J.R. Satti, D.K. Das, D.R. Ray, Measurements of Densities of Propylene Glycol-Based Nanofluids and Comparison With Theory, J. Therm. Sci. Eng. Appl. 8 (2016), https://doi.org/10.1115/1.4032671.
[25] N. Pradeep, K. Paramasivam, T. Rajesh, V. Subash Purusothamanan, S. Iyahraja, Silver nanoparticles for enhanced thermal energy storage of phase change materials, Mater. Today:. Proc. 45 (2021) 607–611, https://doi.org/10.1016/j.matpr.2020.02.671.
[26] Y. Goldberg, M.E. Levinshtein, S.L. Rumyantsev, in: Properties of Advanced Semiconductor Materials GaN, 2001, pp. 93–148.
[27] Beryllium oxide, American Beryllia Inc. (n.d.). https://www.americanberyllia.com/beryllium-oxide (accessed September 8, 2024).
[28] A. Bhattad, S.S. Babu, Thermal analysis of shell and tube type heat exchanger using hybrid nanofluid, Trends in Sciences 19 (2022) 2890. https://doi.org/10.48048/tis.2022.2890.
[29] K. Kulthanan, P. Nuchkull, S. Varothai, The pH of water from various sources: an overview for recommendation for patients with atopic dermatitis, Asia Pac, Allergy 3 (2013) 155–160, https://doi.org/10.5415/apallergy.2013.3.3.155.
[30] D.C.H. Cheng, E. Gulari, Micellization and intermicellar interactions in aqueous sodium dodecyl benzene sulfonate solutions, J. Colloid Interface Sci. 90 (1982) 410–423, https://doi.org/10.1016/0021-9797(82)90308-3.
[31] H. Barabadi, O. Hosseini, K. Jounaki, S. Sadeghian-Abadi, F. Ashouri, A. Mostafa Abdulabbas Alrikabi, H. Vahidi, S. Amidi, F. Mojab, N. Mohammadi, E. Mostafavi, Bioinspired green-synthesized silver nanoparticles: in vitro physicochemical, antibacterial, biofilm inhibitory, genotoxicity, antidiabetic, antioxidant, and anticoagulant performance, Mater Adv 4 (2023) 3037–3054. https://doi.org/10.1039/D3MA00089C.
[32] P. Kumar Kanti, P. Sharma, K.V. Sharma, M.P. Maiya, The effect of pH on stability and thermal performance of graphene oxide and copper oxide hybrid nanofluids for heat transfer applications: Application of novel machine learning technique, Journal of Energy Chemistry 82 (2023) 359–374, https://doi.org/10.1016/j.jechem.2023.04.001.
[33] M.H. Ali, M.A.K. Azad, K.A. Khan, M.O. Rahman, U. Chakma, A. Kumer, Analysis of Crystallographic Structures and Properties of Silver Nanoparticles Synthesized Using PKL Extract and Nanoscale Characterization Techniques, ACS Omega 8 (2023) 28133–28142, https://doi.org/10.1021/acsomega.3c01261.
[34] J. Xu, J. Hu, C. Peng, H. Liu, Y. Hu, A simple approach to the synthesis of silver nanowires by hydrothermal process in the presence of gemini surfactant, J. Colloid Interface Sci. 298 (2006) 689–693, https://doi.org/10.1016/j.jcis.2005.12.047.
[35] X. Wang, R. Wang, C. Peng, T. Li, B. Liu, Synthesis and sintering of beryllium oxide nanoparticles, Prog. Nat. Sci.: Mater. Int. 20 (2010) 81–86, https://doi.org/10.1016/S1002-0071(12)60011-2.
[36] N.M. Sultan, T.M.B. Albarody, H.K.M. Al-Jothery, M.A. Abdullah, H. G. Mohammed, K.O. Obodo, Thermal Expansion of 3C-SiC Obtained from In-Situ X-ray Diffraction at High Temperature and First-Principal Calculations, Materials 15 (2022) 6229, https://doi.org/10.3390/ma15186229.
[37] S. Upadhyay, K. Parekh, B. Pandey, Influence of crystallite size on the magnetic properties of Fe3O4 nanoparticles, J. Alloy. Compd. 678 (2016) 478–485, https://doi.org/10.1016/j.jallcom.2016.03.279.
[38] V. Uvarov, I. Popov, Metrological characterization of X-ray diffraction methods for determination of crystallite size in nano-scale materials, Mater Charact 58 (2007) 883–891, https://doi.org/10.1016/j.matchar.2006.09.002.
[39] M.R. Esfahani, E.M. Languri, M.R. Nunna, Effect of particle size and viscosity on thermal conductivity enhancement of graphene oxide nanofluid, Int. Commun. Heat Mass Transfer 76 (2016) 308–315, https://doi.org/10.1016/j.icheatmasstransfer.2016.06.006.
[40] W. Jin, L. Jiang, Y. Lv, K. Li, H. Liu, W. Cao, C. Chen, Z. Chen, W. Li, Experimental study on preparation and heat transfer efficiency of ethylene glycol/water-based hybrid nanofluids enhanced by graphene oxide/MXene nanoparticles, J. Mol. Liq. 405 (2024) 125033, https://doi.org/10.1016/j.molliq.2024.125033.
[41] H. Babar, H.M. Ali, Towards hybrid nanofluids: Preparation, thermophysical properties, applications, and challenges, J. Mol. Liq. 281 (2019) 598–633, https://doi.org/10.1016/j.molliq.2019.02.102.
[42] V.A. A., D.K. D., A. Idrish Khan, Experimental investigation of thermal conductivity and stability of TiO2-Ag/water nanocompositefluid with SDBS and SDS surfactants Thermochim Acta 678 2019 178308 10.1016/j.tca.2019.178308.
[43] S.-W. Lee, S.-D. Park, S.-R. Kang, S.-M. Kim, H. Seo, D.-W. Lee, I.-C. Bang, Critical heat flux enhancement in flow boiling of Al2O3 and SiC nanofluids under low pressure and low flow conditions, Nucl. Eng. Technol. 44 (2012) 429–436, https://doi.org/10.5516/NET.04.2012.516.
[44] C. Selvam, D. Mohan Lal, S. Harish, Thermophysical properties of ethylene glycol-water mixture containing silver nanoparticles, J. Mech. Sci. Technol. 30 (2016) 1271–1279, https://doi.org/10.1007/s12206-016-0231-5.
[45] L. Li, Y. Zhai, Y. Jin, J. Wang, H. Wang, M. Ma, Stability, thermal performance and artificial neural network modeling of viscosity and thermal conductivity of Al2O3-ethylene glycol nanofluids, Powder Technol. 363 (2020) 360–368, https://doi.org/10.1016/j.powtec.2020.01.006.
[46] R.J. Warzoha, A.S. Fleischer, Determining the thermal conductivity of liquids using the transient hot disk method, Part i: Establishing Transient Thermal-Fluid Constraints, Int J Heat Mass Transf 71 (2014) 779–789, https://doi.org/10.1016/j.ijheatmasstransfer.2013.10.064.
[47] J. Sundberg, G.A. Innova, L. Hälldahl, Comparison of Thermal Properties Measured by Different Methods, Swedish Nuclear Fuel and Waste Management Co (No. SKB-R–03-18) (2003). www.skb.se.
[48] L. Hälldahl, Measurement accuracy and thermal conductivity of water - applications, Hot Disk (2022). https://www.hotdiskinstruments.com/applications/measurement-accuracy-and-thermal-conductivity-of-water/ (accessed January 20, 2024).
[49] J. Lei, Z. Luo, S. Qing, X. Huang, F. Li, Effect of surfactants on the stability, rheological properties, and thermal conductivity of Fe3O4 nanofluids, Powder Technol. 399 (2022) 117197, https://doi.org/10.1016/j.powtec.2022.117197.
[50] K.H. Almitani, N.H. Abu-Hamdeh, S. Etedali, A. Abdollahi, A.S. Goldanlou, A. Golmohammadzadeh, Effects of surfactant on thermal conductivity of aqueous silica nanofluids, J. Mol. Liq. 327 (2021) 114883, https://doi.org/10.1016/j.molliq.2020.114883.
[51] M.U. Sajid, H.M. Ali, Thermal conductivity of hybrid nanofluids: A critical review, Int. J. Heat Mass Transf. 126 (2018) 211–234, https://doi.org/10.1016/j.ijheatmasstransfer.2018.05.021.
[52] M. Sheikholeslami, E. Abohamzeh, Z. Ebrahimpour, Z. Said, Brief overview of the applications of hybrid nanofluids, in, Hybrid Nanofluids, Elsevier (2022) 171–202, https://doi.org/10.1016/B978-0-323-85836-6.00008-9.
[53] M. Hemmat Esfe, S. Saedodin, M. Biglari, H. Rostamian, Experimental investigation of thermal conductivity of CNTs-Al2O3/water: A statistical approach, in: International Communications in Heat and Mass Transfer 69, 2015, pp. 29–33, https://doi.org/10.1016/j.icheatmasstransfer.2015.10.005.
[54] A. Kazemi-Beydokhti, H.A. Namaghi, S.Z. Heris, Identification of the Key Variables on Thermal Conductivity of CuO Nanofluid by a Fractional Factorial Design Approach, Numerical Heat Transfer, Part b: Fundamentals 64 (2013) 480–495, https://doi.org/10.1080/10407790.2013.831674.
[55] J.C. Maxwell, A Treatise on Electricity and Magnetism, Clarendon Press, 1873 https://books.google.com.pk/books?id=92QSAAAAIAAJ.
[56] R.L. Hamilton, O.K. Crosser, Thermal Conductivity of Heterogeneous Two-Component Systems, Ind. Eng. Chem. Fundam. 1 (1962) 187–191, https://doi.org/10.1021/i160003a005.
[57] I.M. Mahbubul, R. Saidur, M.A. Amalina, Influence of particle concentration and temperature on thermal conductivity and viscosity of Al2O3/R141b nanorefrigerant, Int. Commun. Heat Mass Transfer 43 (2013) 100–104, https://doi.org/10.1016/j.icheatmasstransfer.2013.02.004.
[58] A.S. Dalkılıç, G. Yalçın, B.O. Küçükyıldırım, S. Öztuna, A. Akdoğan Eker, C. Jumpholkul, S. Nakkaew, S. Wongwises, Experimental study on the thermal conductivity of water-based CNT-SiO2 hybrid nanofluids, in: International Communications in Heat and Mass Transfer 99, 2018, pp. 18–25, https://doi.org/10.1016/j.icheatmasstransfer.2018.10.002.
[59] I. Kazemi, M. Sefid, M. Afrand, Improving the thermal conductivity of water by adding mono & hybrid nano-additives containing graphene and silica: A comparative experimental study, Int. Commun. Heat Mass Transfer 116 (2020) 104648, https://doi.org/10.1016/j.icheatmasstransfer.2020.104648.
[60] S. Sreekumar, A. Ganguly, S. Khalil, S. Chakrabarti, N. Hewitt, J.D. Mondol, N. Shah, Thermo-optical characterization of novel MXene/Carbon-dot hybrid

nanofluid for heat transfer applications, J. Clean. Prod. 434 (2024) 140395, https://doi.org/10.1016/j.jclepro.2023.140395.
[61] Z. Said, R. Saidur, A. Hepbasli, N.A. Rahim, New thermophysical properties of water based TiO2 nanofluid—The hysteresis phenomenon revisited, Int. Commun. Heat Mass Transfer 58 (2014) 85–95, https://doi.org/10.1016/j.icheatmasstransfer.2014.08.034.
[62] H. Zhang, S. Qing, J. Xu, X. Zhang, A. Zhang, Stability and thermal conductivity of TiO2/water nanofluids: A comparison of the effects of surfactants and surface modification, Colloids Surf A Physicochem Eng Asp 641 (2022) 128492, https://doi.org/10.1016/j.colsurfa.2022.128492.
[63] I.P. Moghadam, M. Afrand, S.M. Hamad, A.A. Barzinjy, P. Talebizadehsardari, Curve-fitting on experimental data for predicting the thermal-conductivity of a new generated hybrid nanofluid of graphene oxide-titanium oxide/water, Physica A 548 (2020) 122140, https://doi.org/10.1016/j.physa.2019.122140.
[64] W. Ajeeb, R.R.S. Thieleke da Silva, S.M.S. Murshed, Experimental investigation of heat transfer performance of Al2O3 nanofluids in a compact plate heat exchanger, Appl. Therm. Eng. 218 (2023) 119321, https://doi.org/10.1016/j.applthermaleng.2022.119321.
[65] X. Shen, X. Sun, J. Liu, J. Hang, L. Jin, L. Shi, A facile strategy to achieve monodispersity and stability of pigment TiO2 particles in low viscosity systems, J. Colloid Interface Sci. 581 (2021) 586–594, https://doi.org/10.1016/j.jcis.2020.07.132.
[66] IAPWS R12-08: Viscosity of Ordinary Water, (2018). http://www.iapws.org/relguide/viscosity.html.
[67] A.V. Minakov, D.V. Guzei, M.I. Pryazhnikov, V.A. Zhigarev, V.Y. Rudyak, Study of turbulent heat transfer of the nanofluids in a cylindrical channel, Int. J. Heat Mass Transf. 102 (2016) 745–755, https://doi.org/10.1016/j.ijheatmasstransfer.2016.06.071.
[68] M. Hemmat Esfe, S. Saedodin, O. Mahian, S. Wongwises, Efficiency of ferromagnetic nanoparticles suspended in ethylene glycol for applications in energy devices: Effects of particle size, temperature, and concentration, in: International Communications in Heat and Mass Transfer 58, 2014, pp. 138–146, https://doi.org/10.1016/j.icheatmasstransfer.2014.08.035.
[69] H. Babar, M. Sajid, H. Ali, Viscosity of hybrid nanofluids: A critical review, Therm. Sci. 23 (2019) 1713–1754, https://doi.org/10.2298/TSCI181128015B.
[70] S.M. Mousavi, F. Esmaeilzadeh, X.P. Wang, A detailed investigation on the thermo-physical and rheological behavior of MgO/TiO2 aqueous dual hybrid nanofluid, J. Mol. Liq. 282 (2019) 323–339, https://doi.org/10.1016/j.molliq.2019.02.100.
[71] A. Mariano, M.J. Pastoriza-Gallego, L. Lugo, L. Mussari, M.M. Piñeiro, Co3O4 ethylene glycol-based nanofluids: Thermal conductivity, viscosity and high pressure density, Int. J. Heat Mass Transf. 85 (2015) 54–60, https://doi.org/10.1016/j.ijheatmasstransfer.2015.01.061.
[72] NIST Chemistry Webbook, SRD 69, Thermophysical Properties of Fluid Systems, (n.d.). https://webbook.nist.gov/chemistry/fluid/ (accessed March 23, 2024).